Physics of Organic Semiconductors, W. Bruetting (Ed.), Wiley-VCH (2005) 95-127 https://doi.org/10.1002/3527606637.ch4

Thermal and Structural Properties of the Organic Semiconductor Alq_3 and Characterization of its Excited Electronic Triplet State

M. Cölle[*1] and **W. Brütting**[**2]

[1] Universität Bayreuth, Experimentalphysik II and Bayreuther Institut für Makromolekülforschung (BIMF), 95440 Bayreuth, Germany
present address: Philips Research Laboratories, 5656 AA Eindhoven, The Netherlands
[2] Universität Augsburg, Experimentalphysik IV, 86135 Augsburg, Germany

Received zzz, revised zzz, accepted zzz
Published online zzz

PACS 33.15.Bh, 33.20.Tp, 33.50.-j, 61.50.-f, 78.20.-e, 85.60.Jb

This review describes the thermal, structural and photophysical properties of different polycrystalline phases of the organic semiconductor Alq_3. In particular the new blue luminescent δ-phase is shown to contain the facial isomer. The results obtained by using differential scanning calorimetry, X-ray diffraction, infrared spectroscopy, transient and delayed photoluminescence measurements clearly demonstrate the existence of this isomer. From the results presented it is now possible to obtain the pure facial isomer of Alq_3 in large quantities, providing the basis for further investigations to determine its effects on the performance of organic light-emitting diodes. Furthermore, recent results on the properties of the triplet states in Alq_3 are presented. This includes the population of the electronic excited triplet state due to intersystem crossing and the spectrum of the phosphorescence.

© 2004 WILEY-VCH Verlag GmbH & Co. KGaA, Weinheim

1 Introduction

8-hydroxyquinoline metal chelate complexes were used for many years in analytical chemistry for a gravimetric determination of various metal cations in solution [1]. The development of more convenient spectroscopic techniques has meanwhile replaced this method and concomitantly decreased the interest of researching chemists in this reagent. Increasing interest in tris(8-hydroxyquinoline)aluminum(III) (Alq_3) shown in Figure 1 for technical applications started with a report on efficient electroluminescent devices using Alq_3 as the active medium [2]. These so-called organic light emitting diodes (OLEDs) opened the way for a new generation of flat panel displays. After nearly two decades of intensive research and development of OLEDs, Alq_3 still continues to be the workhorse in low-molecular weight materials for these devices. It is used as electron-transporting layer, as emission layer where green light emission is generated by electron-hole recombination in Alq_3, and it also serves as host material for various dyes to tune the emission color from green to red [3]. Many studies in this field have focused on the optimization of device performance with respect to efficiency and long-term stability or on the understanding of charge transport properties of amorphous thin films [4-13]. These investigations revealed that electrical transport in Alq_3 is characterized by a hopping-type charge carrier mobility displaying a Poole-Frenkel-like dependence on the electric field and on temperature. It was further found that trapping in distributed trap states is involved in charge transport, in particular at low fields. Different suggestions as to the origin of these traps were made, including a polaronic self–trapping effect, extrinsic traps due to

[*] Corresponding author: e-mail: info@michael-coelle.de, Phone: +31 40 27 42 117, Fax: +31 40 27 43350
[**] e-mail: wolfgang.bruetting@physik.uni-augsburg.de.

Physics of Organic Semiconductors, W. Bruetting (Ed.), Wiley-VCH (2005) 95-127 https://doi.org/10.1002/3527606637.ch4

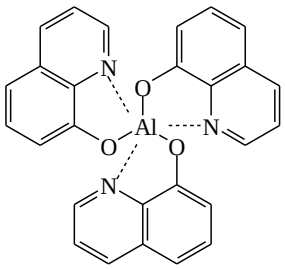

Figure 1: *Chemical structure of Tris(8-hydroxyquinoline)aluminum(III) (Alq_3)*

impurities and the presence of a mixture of isomers of the Alq_3 molecule having different energy levels. However, no clear proof for one or the other possibility explaining the microscopic nature of these traps was given.

Another surprising circumstance was that in spite of the widespread usage of Alq_3 as amorphous films in OLEDs, comparatively few investigations were devoted to the material's structural, electronic and optical properties in the crystalline state, as well as to the dependence of these properties on the preparation conditions until recently [14-17]. On the other hand, it was mentioned in one of the very first publications on OLEDs based on thin films that the so-called "amorphous" film of Alq_3 might have nanocrystalline domains [2], which raises questions concerning the morphology and properties of Alq_3. For example, what kind of crystalline phases can be formed by Alq_3 and what are their electronic and optical properties? What is the packing of the molecules? Packing and intermolecular interactions are important for optical properties as well as for their electrical characteristics and the transport mechanism of charge carriers.

Another unresolved issue concerns the isomerism of the Alq_3 molecule. It is well-known that octahedral complexes of the type MN_3O_3, where M is a trivalent metal and N and O stand for the nitrogen and oxygen atoms in the quinoline ligands, can occur in two different geometric isomers: meridional and facial,

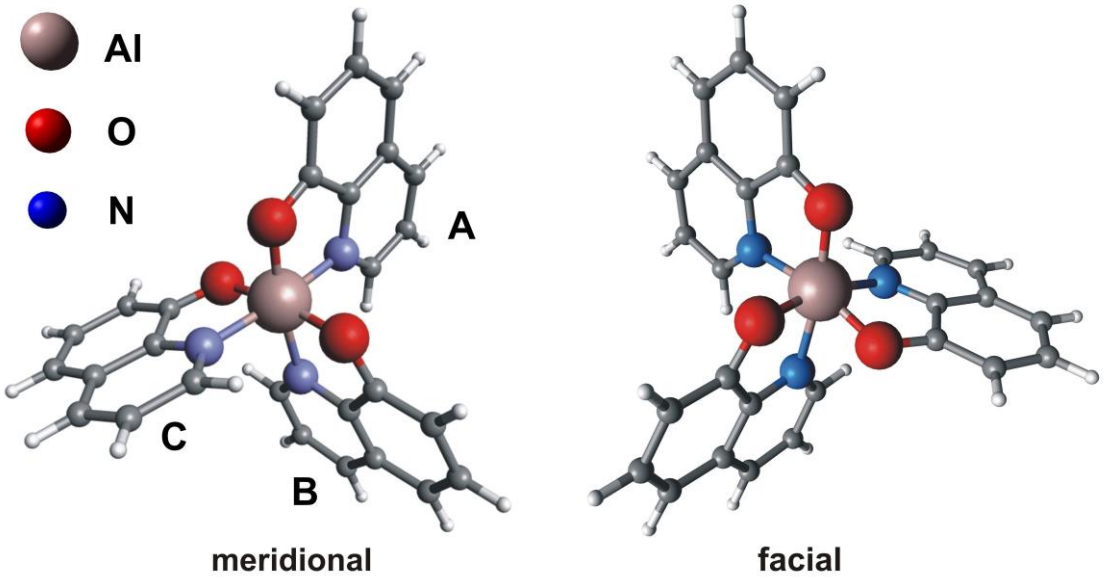

Figure 2: Molecular structure of the meridional and facial isomer of Alq_3. For the facial isomer the ligands are equivalent, but in the meridional molecule the ligands can be clearly distinguished and therefore the labeling of the ligands by A, B and C is given.

Physics of Organic Semiconductors, W. Bruetting (Ed.), Wiley-VCH (2005) 95-127 https://doi.org/10.1002/3527606637.ch4

as shown in Figure 2 [18]. Nevertheless, until recently only the meridional isomer had been clearly identified and no direct experimental evidence for the facial isomer had been found. Therefore it was generally believed that the meridional isomer is predominant, both in amorphous films and crystals of Alq_3. The existence and the properties of the facial isomer are discussed in detail in the literature and a key issue is its possible presence in sublimed Alq_3 films [14,19-27]. Many suggestions have been made about its influence on trap density, charge carrier transport and thus on the characteristics and performance of OLEDs. For example, the higher dipole moment of the facial isomer is expected to influence the morphology of the film as well as the injection of charge carriers at the interface. In addition the different HOMO and LUMO levels predicted for the two isomers are expected to influence the injection barrier and could act as traps for charge carriers [24,28-32]. Therefore the question is whether the facial isomer is present in one or the other modification of Alq_3, and if so, if it is possible to isolate it. The isolation of the facial isomer is of great interest, as it will allow its properties to be examined separately and thus its role in OLEDs to be clarified.

Crystalline Phases of Alq_3

This section describes the preparation and identification of different crystalline phases of Alq_3 obtained by sublimation. In order to induce growth of different phases, the temperature gradient in a sublimation tube was used. Phases that grow at different temperatures were obtained and their crystal structures were investigated.

Temperature gradient sublimation is a common method for purification of organic materials. After this purification procedure polycrystalline powders of different appearance were found in the sublimation tube and thus we distinguished between three different zones in the glass tube. The materials in these zones, hereafter called fractions, differ in their shape of crystals, their color, their solubility and their fluorescence.

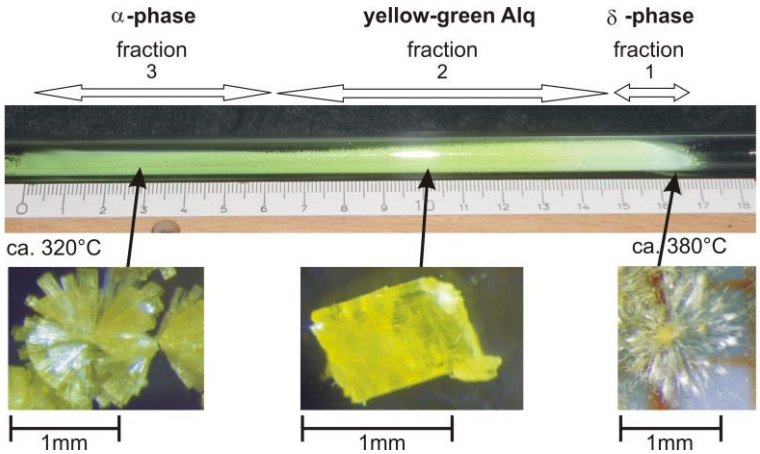

Figure 3: *Picture of a sublimation tube. Due to the temperature gradient in the sublimation tube, the material obtained is separated into three zones, which are labeled by fraction 1, fraction 2 and fraction 3. Crystals of these fractions in the tube are also shown.*

Physics of Organic Semiconductors, W. Bruetting (Ed.), Wiley-VCH (2005) 95-127 https://doi.org/10.1002/3527606637.ch4

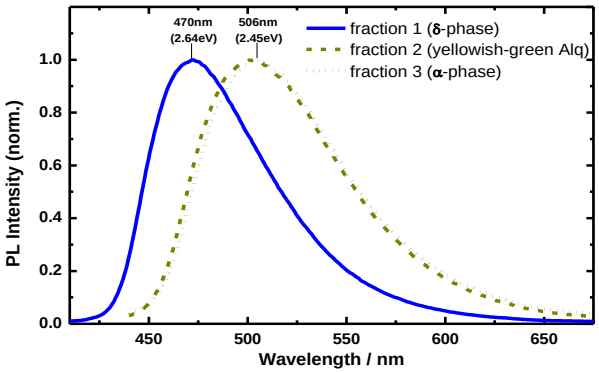

Figure 4: *PL spectra of the three fractions obtained from the sublimation tube, excited at 350nm and measured at room temperature.*

A typical example of these glass tubes after sublimation is shown in Figure 3 with indicated areas for the three different fractions. In the hottest zone of the growth area there is an approximately 1.5cm wide region with very small needle-like crystals with white or slightly yellow appearance (fraction1). This zone is followed by the main fraction (about 8.5cm) with yellow cubic crystals and dimensions up to 500x500x500μm^3, showing yellowish-green fluorescence (fraction2). In the subsequent colder zone of the sublimation tube another fraction is obtained with dark yellow-green needle-like crystals with a size of 50x50x500μm^3 (fraction 3).

These fractions have different solubility in organic solvents. While fraction 3 and (apart from a small residue) also fraction 2 are readily dissolved in chloroform at a relatively high concentration of more than 1% by weight, the solubility of fraction 1 is extremely poor. It takes several hours to dissolve a

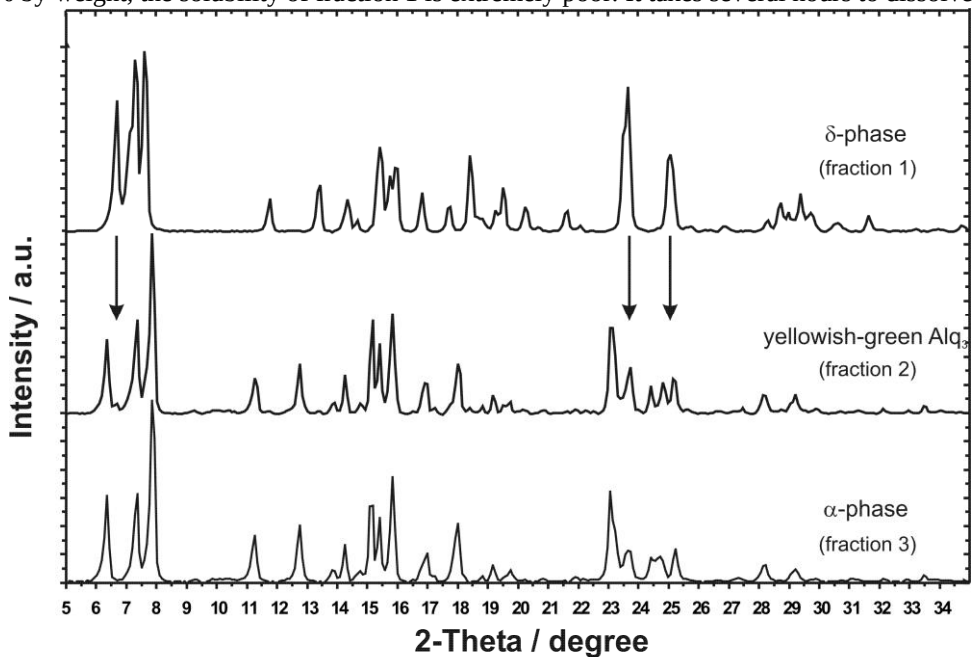

Figure 5: *X-ray powder diffractograms of polycrystalline Alq_3 fractions 1, 2, and 3 obtained from the sublimation tube in the 2Θ-range from 5 to 35 degrees (step width Δ2Θ=0.083°). Arrows mark areas with the most significant differences.*

Physics of Organic Semiconductors, W. Bruetting (Ed.), Wiley-VCH (2005) 95-127 https://doi.org/10.1002/3527606637.ch4

Table 1: Crystallographic data of the polycrystalline phases of Alq_3.

	α-phase (fraction 3) [14, 15]	β-phase [14]	γ-phase [14]	δ-phase (fraction 1) [16, 17]
crystal system	triclinic	triclinic	trigonal	triclinic
space group	P-1	P-1	P-31c	P-1
Z	2	2	2	2
a [Å]	12.91	10.25	14.41	13.24
b [Å]	14.74	13.17	14.41	14.43
c [Å]	6.26	8.44	6.22	6.18
α [°]	89.7	97.1	90	88.55
β [°]	97.7	89.7	90	95.9
γ [°]	109.7	108.6	120	113.9
V [$Å^3$]	1111	1072	1118	1072.5

sizeable amount in chloroform, but then the color of the solution becomes similar to that of the other fractions.

Further differences between the three fractions are found in their photoluminescence (PL) spectra. Figure 4 shows the spectra measured with an excitation wavelength of 350nm at room temperature. All fractions show one broad PL band with no additional structures and a tail at the side of longer wavelengths. Their main difference is the large blue shift of the PL maximum of about 0.19eV (36nm) from fraction 3 to fraction 1 with a PL maximum at about 506nm (2.45eV) and 470nm (2.64eV), respectively.

In order to investigate the origin of these differences, the crystallographic data of the three fractions were determined by using X-ray powder diffraction as shown in Figure 5. As a result two different phases were found. Fraction 1 and fraction 3 show the main differences. These differences are best seen for small angles below 9 degrees and in the region between 22 and 26 degrees. From these two spectra the unit cells for fraction 1 and fraction 3 were determined. Indexing of the peaks observed is given in Reference [15] and [17] and the cell parameters determined for the different phases of Alq_3 are summarized in Table 1 together with two other phases (β- and γ-) found by Brinkmann et al. The spectrum of fraction 2 seems to be a mixture of two phases. Basically the spectrum is similar to that of fraction 3 apart from some small peaks or shoulders at positions where fraction 1 and fraction 3 are different, for example at 23.5 degrees and especially at 6.69 degrees. This suggests that fraction 2 mainly consists of the same phase as fraction 3, but has some small admixtures of material from fraction 1. The result that fraction 2 is a mixture of two different phases is relevant for applications, as it is mainly this fraction that is used for fabrication of OLEDs. From these X-ray data it becomes clear that the main difference is between fraction 1 and fraction 3, which have different unit cells given in Table 1.

It is possible to compare these crystal data obtained above with results of other researchers. Brinkmann et al. reported on three different crystalline structures called α-, β- and γ-phase [14]. The published data for the α-phase are identical to those of fraction 3. β-Alq_3 is grown from solution and its properties are in principle similar to the α-phase, only with a small red shift in the PL due to slightly different intermolecular interaction in the crystal. The published data of γ-Alq_3 are listed in Table 1 for completeness. All phases and evaporated films were identified as consisting of the meridional isomer, and therefore only the meridional molecule was found at that time.

The denotation of the phases in our work is in accordance with these published data. Fraction 3 and the main part of fraction 2 consist of the α-phase. The structure of fraction 1 is new and no corresponding phase has been published so far. Accordingly fraction 1 is hereafter called the δ-phase of Alq_3.

δ-Alq_3 exhibits major differences to all other phases obtained from the sublimation tube. It is a whitish powder, has a different crystal structure and, importantly, a strongly blue-shifted PL. On the other hand the α- and β- phase are very similar, as reported by Brinkmann et al. Consequently it seems to be most

Physics of Organic Semiconductors, W. Bruetting (Ed.), Wiley-VCH (2005) 95-127 https://doi.org/10.1002/3527606637.ch4

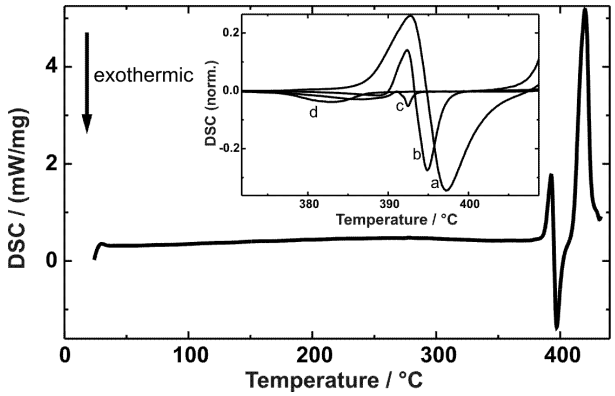

Figure 6: DSC trace of Alq_3 with pronounced thermal transitions at 393°, 396° and 419°C measured at a heating rate of 20°C/min. Inset: Broadening and intermingling of the endothermic and exothermic peaks around 395°C in the DSC signal related to the sweep speed (a: 20°C/min, b: 10°C/min, c: 5°C/min, d: 2°C/min; normalized on the melting peak intensity). At low measuring speed only the more pronounced exothermic transition is visible.

interesting to investigate the differences and similarities of the α- and δ- phase of Alq_3, as will be done in the following sections of this article.

Thermal Properties of Alq_3

The phases discussed above were grown in different areas of the sublimation tube in regions of different temperature. Thus temperature obviously has a strong influence on the formation of these phases and it is important to learn more about the thermal properties of Alq_3. Therefore the formation conditions of the different phases of Alq_3 were investigated using differential scanning calorimetry (DSC) measurements in combination with structural and optical characterization.

Figure 6 shows the DSC measurement of polycrystalline Alq_3 powder (α-phase) taken at a heating rate of 20°C/min. Coupled endothermic and exothermic peaks are observed at about 395°C prior to the large melting transition at 419°C. This additional phase transition has also been reported in the literature and has been attributed to polymorphism of the crystalline material [14, 34]. It is very pronounced at fast heating rates (above 15°C/min). For slow heating rates the endothermic and exothermic transitions become broader and the peak height decreases as compared to the strong melting peak. The peaks start to intermingle and are shifted to a slightly lower temperature, as shown in the inset of Figure 6 for heating rates of 20°, 10°, 5° and 2°C per minute. This behavior is similar to known irreversible monotropic solid-solid transitions [35-37]. Typically, the monotropic transition is slow and is mostly observed a few degrees below the melting point. Thus it is advisable to measure the monotropic transition isothermally at very slow heating rates.

It should be noted that increasing the temperature above 430°C results in decomposition of the material and that a small broad transition at 320°C reported by Sapochak et al. [34] was not observed in our samples. For the following measurements a slow heating rate of 2°C/min was used, where the shift of the peak temperatures is fairly small (see Figure 6) and where it is possible to stop the process at a defined temperature. Using this procedure the conditions for the preparation of different Alq_3 phases by a controlled thermal annealing process were investigated.

For these slow DSC measurements three different regions are distinguished in Figure 7: In the first region (A) below the exothermic phase transition Alq_3 is the usual yellowish green powder, in the second region (B) between this phase transition and the melting peak Alq_3 is a whitish powder, and finally in region C Alq_3 is a liquid melt. The glassy state of Alq_3 was obtained by quenching this melt in liquid nitrogen. Its highly amorphous character was verified by using X-ray powder diffraction measurements

Physics of Organic Semiconductors, W. Bruetting (Ed.), Wiley-VCH (2005) 95-127 https://doi.org/10.1002/3527606637.ch4

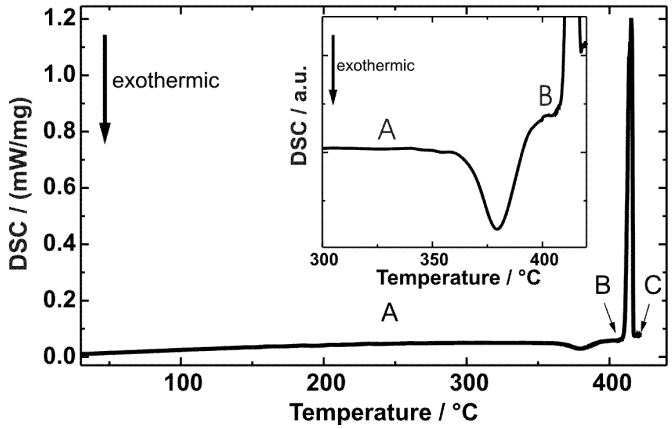

Figure7: DSC trace of Alq_3 measured at a heating rate of 2°C/min. The clearly pronounced exothermic phase transition at 380°C prior to the melting point is enlarged in the inset, as it becomes broad and less intense compared to the melting peak for this slow heating rate. A, B and C mark the regions of yellowish-green Alq_3, blue Alq_3 and melt, respectively.

with an image plate detection system. Cooling down the liquid melt slowly resulted in yellowish-green powder (A) again, as was previously reported [38]. All of these materials are stable at room temperature. Figure 8 shows the PL spectra measured at room temperature of annealed polycrystalline Alq_3 powder from regions A and B as well as of the quenched amorphous melt (C). For annealing temperatures up to 365°C Alq_3 is a yellowish-green powder with a PL maximum at 506nm (curve A). After the exothermic transition at about 380°C, there is a big blue shift of 0.18eV (37nm), associated with a slight change in the shape of the PL spectrum (curve B), which is less symmetric for blue Alq_3. The quenched melt (curve C) is clearly red-shifted (0.14eV) compared to the yellowish-green Alq_3-powder (curve A). The strong difference in the emission color can be seen in Figure 9, where samples of the quenched melt, yellowish-green and blue Alq_3 are shown in daylight (a) and under UV-irradiation (b), respectively. The emission color is shifted from green (CIE coordinates: x=0.27, y=0.5) to blue (x=0.16, y=0.26). From Figure 9 one can also see the relatively low PL intensity of the quenched melt compared to the very intense PL emis-

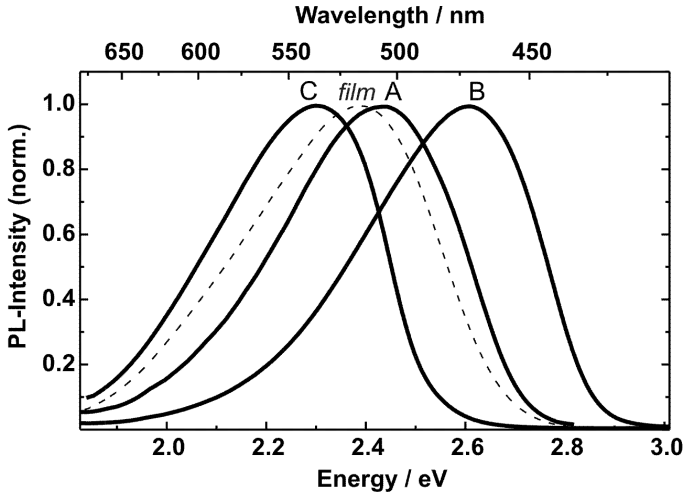

Figure 8: *PL spectra of Alq_3 samples taken from regions A, B and C of* Figure 7*, respectively, excited at 350nm. The PL of an evaporated Alq_3 film (dashed line) is shown for purposes of comparison. All spectra were measured at room temperature.*

Physics of Organic Semiconductors, W. Bruetting (Ed.), Wiley-VCH (2005) 95-127 https://doi.org/10.1002/3527606637.ch4

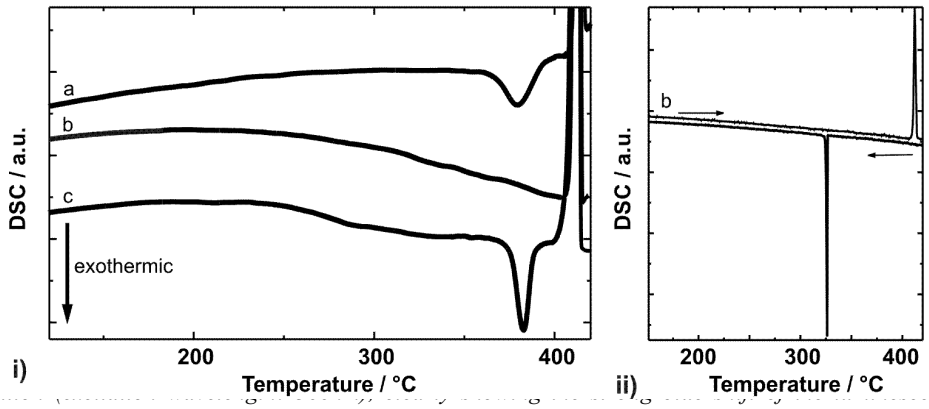

annealed material (CIE color coordinates for A: x=0.27, y=0.50; for B: x=0.16, y=0.26).

Figure 10: DSC traces of a: yellowish-green Alq_3 and b: blue Alq_3. Trace c shows a second heating cycle after cooling down the melt (b) again. By annealing blue Alq_3 no phase transition at 380°C is observed (trace b in i) and ii)). Cooling down the melt gives a strong recrystallization peak.

sion of blue Alq_3. For PL quantum efficiency the values obtained for blue Alq_3, yellowish-green powder, evaporated film and quenched amorphous melt were 51%, 40%, 19% and 3%, respectively.

For comparison the dashed line in Figure 8 is the PL spectrum of an evaporated Alq_3-film as used in OLEDs. Although these films are commonly called "amorphous", one can clearly see that the PL maximum is located between the quenched melt and crystalline Alq_3. This is an indication of the nanocrystalline character of these films, as noted already by Tang et al. [2].

Yellowish-green Alq_3, blue Alq_3 and amorphous melt can be converted into each other. As described above, yellowish-green Alq_3 annealed above the phase transition at 380°C results in blue Alq_3. Annealing blue Alq_3 above the melting point and cooling it down slowly, as shown in Figure 10, yields yellowish-green powder again and a pronounced recrystallization peak is observed. With the same procedure of annealing the quenched melt above the melting point and cooling it down slowly, yellowish-green powder is obtained again, and the quenched melt is converted into blue Alq_3 by annealing it between 380°C and 410°C. The successful conversion from one phase into the other was confirmed by measurements of the PL spectra, FT-IR spectra, Raman spectra, and X-ray diffraction.

Obviously, blue Alq_3 is formed during the phase transition at about 380°C. This phase transition appeared when starting the measurement with yellowish-green Alq_3, as shown in Figure 10. On the other hand, when starting the annealing procedure with blue Alq_3 material no such phase transition was observed, as shown in Figure 10 i) and ii) trace b. However, measurements taken after the sample in Figure 10 b had cooled down showed the exothermic peak again, as can be seen in trace c of Figure 10 i).

As blue Alq_3 is formed in the region between the crystallographic phase transition and the melting point, the influence of temperature and preparation conditions in the region between 385°C and 410°C was investigated. Figure 11 shows X-ray powder diffraction spectra of blue Alq_3 prepared under three different conditions. For spectrum (I) yellowish-green Alq_3 powder (α-Alq_3) was annealed at 400°C for 2h. This spectrum is similar to the one obtained for fraction 1 in the sublimation tube shown in Figure 5. The shoulder at 2θ=7.05° for different samples of blue Alq_3 was variably pronounced. From this one may assume another high-temperature phase to be present in these samples. To test this, Alq_3 was annealed for several minutes at a higher temperature of 410°C (very close to the melting point) and a dark yellow substance was obtained, which exhibited only poor photoluminescence together with blue luminescent material. Its X-ray spectrum (Figure 11 (II)) has a number of new peaks, which become very obvious for example at 2Θ=7.05° (the position of the shoulder in spectrum (I)) and 25.85°. On the other hand, spectrum (III) shows Alq_3-powder annealed at 390°C for 6 hours. The additional lines observed in spectrum (II) are no longer present in this spectrum.

Physics of Organic Semiconductors, W. Bruetting (Ed.), Wiley-VCH (2005) 95-127 https://doi.org/10.1002/3527606637.ch4

Based on these investigations, blue luminescent Alq_3 obtained by annealing yellowish-green Alq_3 (α-phase) above the phase transition at about 380°C was identified as the δ-phase of Alq_3 with the unit cell given in Table 1. As seen in curves (I) and (II) of Figure 11, annealing Alq_3 at temperatures higher than 380°, close to the melting point, results in the appearance of new peaks in the X-ray spectra, which can be attributed to an additional high temperature phase. Brinkmann et al. have reported on such a high temperature phase, namely γ-Alq_3 [14]. Using the given unit cell parameters from their work, the positions of all possible X-ray peaks for this phase were calculated, as indicated by the vertical bars in curve (II) of Figure 11. These calculated peaks are located at the positions where spectrum (II) and (III) are different. Therefore it suggests that in sample (II) there is a high concentration of γ-Alq_3, whereas sample (III) is practically pure δ-Alq_3, as will be confirmed in the next section. From this it can be concluded that there are two high temperature phases of Alq_3: δ-Alq_3 and the γ-phase.

Blue luminescent Alq_3 obtained by train sublimation as described in the previous section and by annealing showed the same behavior with respect to its solubility as well as its properties in PL, DSC, and IR measurements, confirming that in both cases the δ-phase of Alq_3 was obtained. In the sublimation tube the different phases were separated due to the temperature gradient. Since δ-Alq_3 and the other high temperature phase (most likely γ-Alq_3) are formed in a relatively narrow temperature region, the separation of the two phases by train sublimation is difficult and a certain ratio of γ-Alq_3 is still present in the samples of δ-Alq_3, as indicated by the small shoulder at 2θ=7.05° in the X-ray spectrum. On the other hand, under appropriate annealing conditions it is possible to obtain pure δ-phase without any visible admixtures of other phases, as demonstrated in curve (III) of Figure 11. A further advantage of this simple annealing process compared to temperature gradient sublimation is the possibility of obtaining large amounts (several grams) of pure δ-Alq_3 in a well-controlled process.

The relative content of δ- and γ- Alq_3 very critically depends on the preparation conditions (e.g. vacuum/atmosphere and temperature) as can also be seen in Figure 11 and can thus be tuned at will choosing suitable parameters. The samples measured in Figure 11 (III) and Figure 12 consist of more than 98% of δ- Alq_3, as can be derived from our X-ray data [67].

Physics of Organic Semiconductors, W. Bruetting (Ed.), Wiley-VCH (2005) 95-127 https://doi.org/10.1002/3527606637.ch4

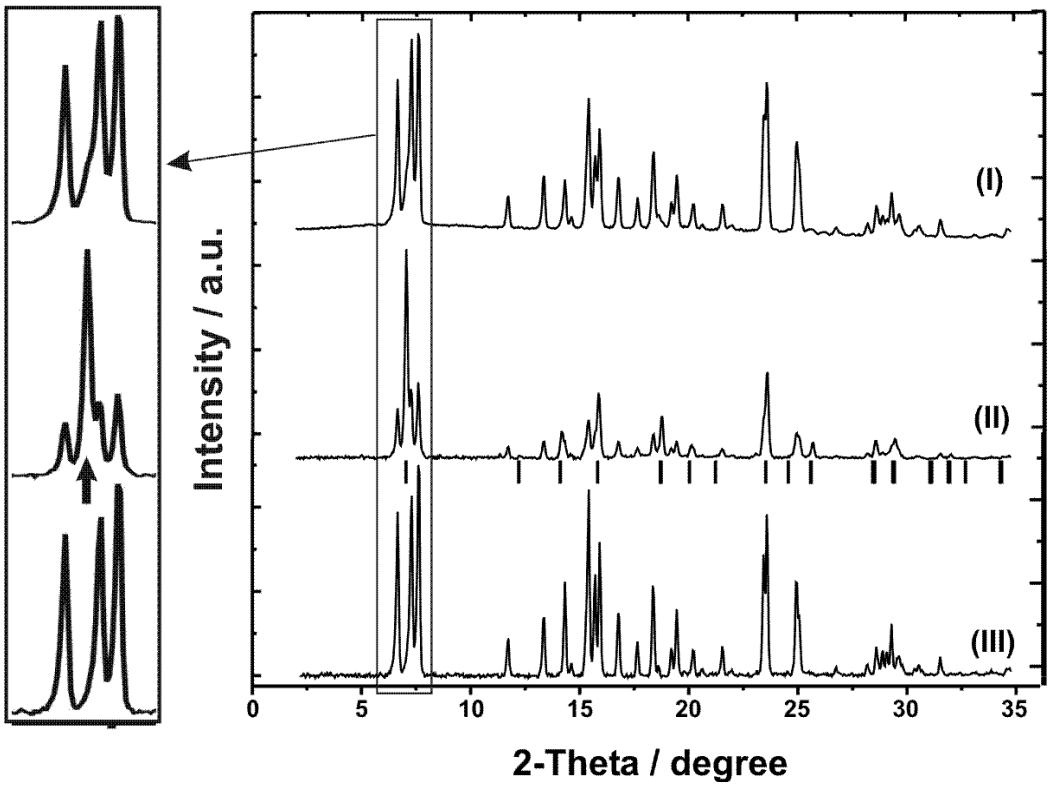

Figure 11: X-ray powder diffractograms of polycrystalline blue Alq_3 prepared under different conditions. For spectrum (I) yellowish-green Alq_3-powder (α-Alq_3) was annealed at 400°C for 2 hours. In spectrum (II) the powder was annealed at 410°C (close to melting point). For spectrum (III) Alq_3 was annealed at 390°C for 6 hours. The additional lines and shoulders observed in spectrum (II) are not present in spectrum (III). Bars in spectrum (II) mark calculated positions for all possible X-ray peaks of γ-Alq_3.

Chemical reactions during the annealing process can be excluded because the usual yellowish-green Alq_3 (α-phase) and the blue luminescent δ-Alq_3 can be easily converted into each other. Annealing yellowish-green Alq_3 at temperatures higher than 380°C results in δ-Alq_3, while heating δ-Alq_3 above the melting point and cooling the melt down slowly results in yellowish-green powder again. Another method of reconverting blue Alq_3 into yellowish-green Alq_3 is to evaporate the material or to dissolve it in any appropriate solvent (e.g. chloroform). The same holds for the glassy state of Alq_3 obtained by quenching the melt. It is readily dissolved in chloroform and films of good quality can be cast from such solutions. The PL spectrum of such films is the same as for evaporated films of Alq_3. By annealing material in the glassy state, it is possible to obtain both the yellowish-green α-Alq_3 and the blue δ-Alq_3, depending on the temperature. In all cases pure Alq_3 with no visible contaminating material is obtained. The possibility of transforming Alq_3 from one phase into the other implies that even at these high temperatures there is no decomposition or chemical reaction of the material. So it is important to emphasize that for all temperatures up to 425°C we are dealing with Alq_3, in agreement with ^{1}H NMR and FT-IR analysis of Alq_3 annealed at 422°C, where no decomposition products have been found [34]. By excluding chemical reactions the difference in the phases must be of physical and structural origin.

Physics of Organic Semiconductors, W. Bruetting (Ed.), Wiley-VCH (2005) 95-127 https://doi.org/10.1002/3527606637.ch4

The Molecular Structure of δ-Alq_3

High resolution powder diffraction using synchrotron radiation

In the previous sections a new phase of Alq_3, the δ-phase, which exhibits major differences to all other phases, was introduced and characterized. Based on the observed blue-shift of the PL by almost 0.2eV and the quantum chemical calculations of Curioni et al., which predicted a difference in the energy gap of the two isomers in that range [28], it could be supposed that the δ-phase contains the facial isomer of Alq_3. However, to prove this hypothesis it was necessary to resolve the crystal structure of the new phase, including the structure of the constituting molecules. The problem in determining the structure of organic molecular crystals is mainly due to the large number of atoms (104 for Alq_3) in the unit cell. Standard laboratory equipment requires single crystals to solve the structure of a new phase of a material; however, so far single crystals large enough for a full analysis of the structure have only been available for the β-phase of Alq_3 [14]. On the other hand, due to the use of high brilliance synchrotron radiation sources powder diffraction methods have progressed substantially in recent years, allowing very reliable determination of the structure from powder material without the need for larger single crystals. For this, high quality experimental data and specialized software for the analysis of the structure are required. These methods are very sensitive and unambiguous results are only to be expected if samples of one uniform crystal phase are measured. As the δ-phase can be isolated and δ-Alq_3 is easily obtained as a fine polycrystalline powder, these are good preconditions for this method.
In the case of a molecular crystal like Alq_3 it is necessary to start the simulation of the spectrum with an assumed configuration of the molecules within the unit cell in order to achieve convergence within a reasonable calculation time. Therefore we assumed a molecular configuration on the basis of the known connectivity of the molecule. The ligands were assumed to be planar and were randomly moved within a range of ±20° by a simulated annealing procedure until a minimal difference to the measured spectrum was obtained. After this, the position of the atoms was optimized by Rietveld refinements [39]. The accuracy of the structure obtained is given by the R-values and the goodness of fit χ. More information on the experimental procedure and analysis is found in Ref. [16] as well as in the literature [40, 43-45].
The following analysis of the data of the δ-phase of Alq_3 was made on the assumption that one of the two isomers is the constituent of this phase. First the results for the facial isomer are given, followed by the results for the meridional isomer for comparison.

Figure 12 shows the spectrum observed together with the best Rietveld-fit profiles for the assumption of the facial isomer. The enlarged difference curve between observed and calculated profiles is given in an

Table 2: *Crystallographic data for δ-Alq_3. R_p, R_{wp}, and R-F^2 refer to the Rietveld criteria of the fit for profile and weighted profile respectively, defined by Langford and Louer [40].*

Formula	$Al(C_9H_6NO)_3$	ρ-calc [g/cm^3]	1.423
Temperature [K]	295	2Θ range [°]	4-35.7
Formula weight [g/mol]	918.88	Step size [°2Θ]	0.005
Space group	P-1	Wavelength [Å]	1.14982(2)
Z	2	μ [1/cm]	2.48
a [Å]	13.2415(1)	Capillary diameter	0.7
b [Å]	14.4253(1)	R_p [%]	5.0
c [Å]	6.17727(5)	R_{wp} [%]	6.5
α [°]	88.5542(8)	R-F^2 [%]	10.5
β [°]	95.9258(7)	Reduced χ^2	1.6
γ [°]	113.9360(6)	No. of reflections	337
V [$Å^3$]	1072.52(2)	No. of variables	115

Physics of Organic Semiconductors, W. Bruetting (Ed.), Wiley-VCH (2005) 95-127 https://doi.org/10.1002/3527606637.ch4

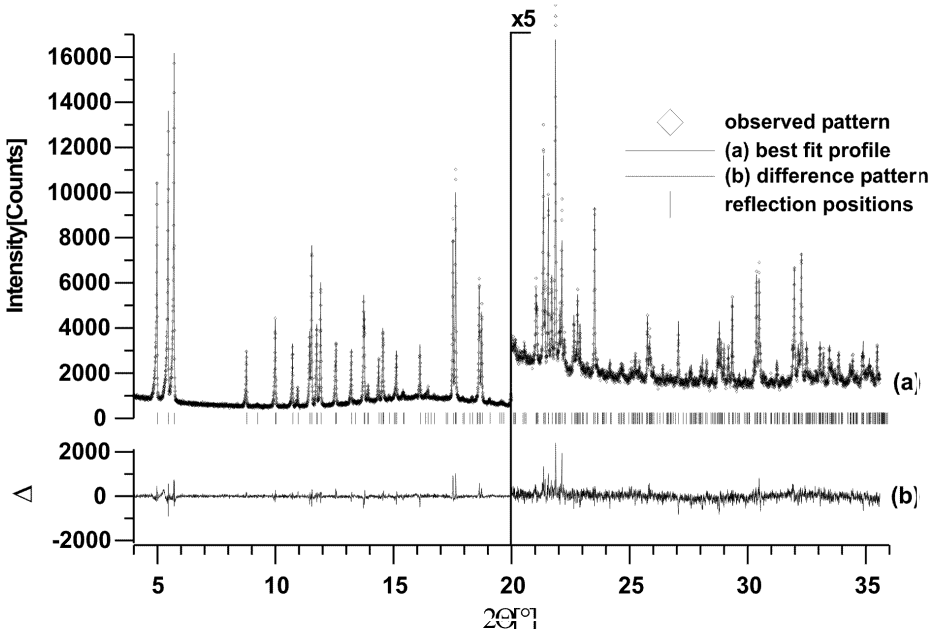

Figure12: *Scattered X-ray intensity for δ-Alq_3 under ambient conditions as a function of diffraction angle 2Θ. Shown are the observed patterns (diamonds), the best Rietveld-fit profiles on the assumption of a facial isomer (line) and the enlarged difference curves between observed and calculated profiles in an additional window below. The high angle part is enlarged by a factor of 5, starting at 20°. The wavelength was λ = 1.15 Å.*

additional window below. Indexing of this very well resolved powder spectrum with the ITO routine [46] led to a primitive triclinic unit cell for Alq_3 with lattice parameters given in Table 2. The number of formula units per unit cell could be determined as Z=2 from packing considerations and density measurements. P-1 was selected as the most probable space group, which was confirmed by Rietveld refinements. The high quality of the refinement becomes obvious from the excellent differential pattern in particular at high diffraction angles (corresponding to small distances in real space), the R_{wp} value of 6.5%, and the Bragg R value R-F^2 of 10.5%. Crystallographic data for δ-Alq_3 are listed in Table 2.

The molecular structure of δ-Alq_3 obtained from these measurements is shown in Figure 13. Compared to the idealized isolated facial Alq_3 isomer, the molecule is only slightly distorted, which reduces its symmetry only negligibly, and the planes defined by the O- and N-atoms, respectively, are parallel. The molecules form linear stacks in the c-direction of the crystal. The projection along the c-axis as well as the projection perpendicular to the planes of the hydroxyquinoline ligands, which shows the overlap between ligands of neighboring Alq_3 molecules, are shown in Figure 14.

The data was also evaluated on the assumption of the meridional isomer. The best fit obtained for this case is plotted in Figure 15 together with the differential curve. A comparison with Figure 12 clearly shows that the fit assuming the meridional isomer is far worse than the result for the facial isomer. Refinement resulted in a distorted meridional molecule, whereby the distance for one coordination bond (Al-N) was elongated more than 10% compared to the others (ligand A and B: ca. 2.1Å, ligand C: 2.39Å) and a Bragg R value R-F^2 of 19.4% was obtained. R-Values, tables and a picture of the distorted meridional molecule are given in Ref.[16] and Ref. [52] .

The most important outcome of these refinements is that the δ-phase of Alq_3 consists of the facial isomer. For a long time it was believed that the facial isomer is unstable and would not exist. Thus the re-

Physics of Organic Semiconductors, W. Bruetting (Ed.), Wiley-VCH (2005) 95-127 https://doi.org/10.1002/3527606637.ch4

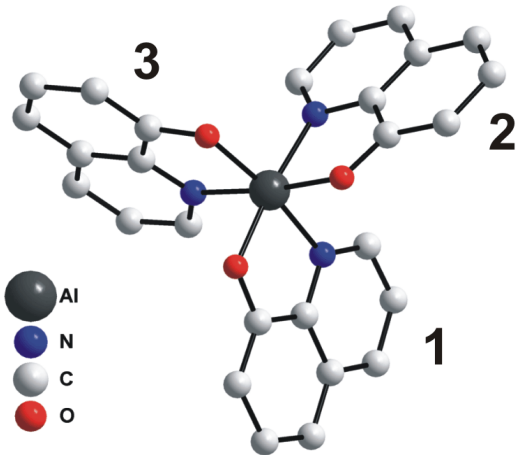

Figure 13: *Facial Alq_3 molecule of the δ-phase with the three hydroxyquinoline ligands labeled by 1, 2 and 3. H-atoms are omitted for simplicity.*

sults shown here give clear evidence for the existence of this facial isomer [16, 47]. The simulations assuming the facial isomer closely match the measured spectrum, as can be seen in the differential spectrum in Figure 12, which is much better than the differential spectrum in Figure 15 of the best possible fit for the meridional isomer. For the meridional isomer the molecule is distorted and a substantially higher Bragg R value (by 9%) was obtained compared to the facial isomer ($R\text{-}F^2$= 10.5% facial, 19.4% meridional). The R values for the facial isomer indicate a high quality of the refinement, resulting in a very high probability that the δ-phase consists of this isomer. Furthermore, the high quality of the fit and the very well resolved spectrum suggests that the samples of δ-Alq_3 are an almost pure phase, confirming the results in the previous section. Therefore it can be concluded that the δ-Alq_3 samples prepared under defined annealing conditions as described above are a pure phase without significant admixtures of other phases and that δ-Alq_3 consists of the facial isomer. Thus, as a result of the preparation of δ-Alq_3, we have for the first time successfully isolated the long sought-after facial isomer of Alq_3.
This assignment of the facial isomer as being the only constituent of the δ-phase of Alq_3 was also very recently confirmed by NMR measurements [50] where the different electric field gradient tensors for the two isomers give characteristic fingerprints for their identification in solid state Al-NMR spectra. Moreover, the group at Eastman Kodak has recently grown single crystals of δ-Alq_3 large enough for a single crystal structure analysis. An excellent confirmation of the structure and the packing presented here was obtained [51].

The data also gives information about distance and orientation of the molecules and thus about molecular packing in the crystal. It is noteworthy that the molecules are arranged in a manner minimizing the possible overlap of the π-orbitals between pairs of hydroxyquinoline ligands belonging to neighboring Alq_3 molecules, as shown in Figure 14. As demonstrated by Brinkmann et al., the orbital overlap influences the optical properties and can explain shifts in the photoluminescence spectra of different phases of Alq_3 [14]. In δ-Alq_3 the pyridine rings of antiparallel ligands 1 face each other with an interligand distance of 3.4Å (Figure 14 (a)). The partial overlap of the rings is smaller than in the other known phases, and the atoms are slightly displaced, further reducing the overlap of the π-orbitals. Figure 14 (b) and (c) show the projection perpendicular to the planes of ligand 2 and ligand 3, respectively. The interligand distance is about 3.45 Å and these ligands do not overlap at all. Thus a strongly reduced π-orbital overlap of neighboring ligands is found in δ-Alq_3 as compared to the α- and β-phase. As only one ligand of each molecule overlaps with a neighboring molecule, there are no π-π links generating an extended one-

Physics of Organic Semiconductors, W. Bruetting (Ed.), Wiley-VCH (2005) 95-127 https://doi.org/10.1002/3527606637.ch4

dimensional chain, as reported for the β-phase [14]. In view of this, both the packing effect with reduced intermolecular interaction and the changed symmetry of the molecule are likely to be responsible for the large blue-shift of the photoluminescence by 0.2eV, which is in the same range as predicted theoretically by Curioni et al. for the two isomers [28].

For transformation from the meridional isomer to the facial isomer one ligand, namely ligand C in Figure 2, has to flip by 180°. From our results the facial isomer is formed at temperatures above 380°C; thus the question is of interest whether this transition is energetically allowed for this molecule. Amati et al. made theoretical calculations for several possible transition processes between the geometric isomers of Alq_3 and its stereoisomers, and they found that thermal conversion from the meridional isomer to the facial isomer is energetically possible [48]. Very recently Utz et al. reported on NMR measurements of solutions demonstrating an internally mobile nature of the Alq_3 complex [49]. They found a high probability of ligands flipping by 180° and suggested that this process takes place on a time scale of about $5s^{-1}$ at room temperature in solution. In these measurements they were only able to determine the meridional isomer for two reasons: First, the facial isomer is predicted to be less stable by about 17kJ/mol for the isolated molecule [28, 48], thereby reducing its lifetime in solution; second, only the flip of ligand C may result in the facial isomer, giving a lower probability for this process, and thus the expected concentration of this isomer in solution is likely to be too small to be measured [49]. These measurements and the theoretical work of Amati et al. demonstrate that the transformation from the meridional isomer to the

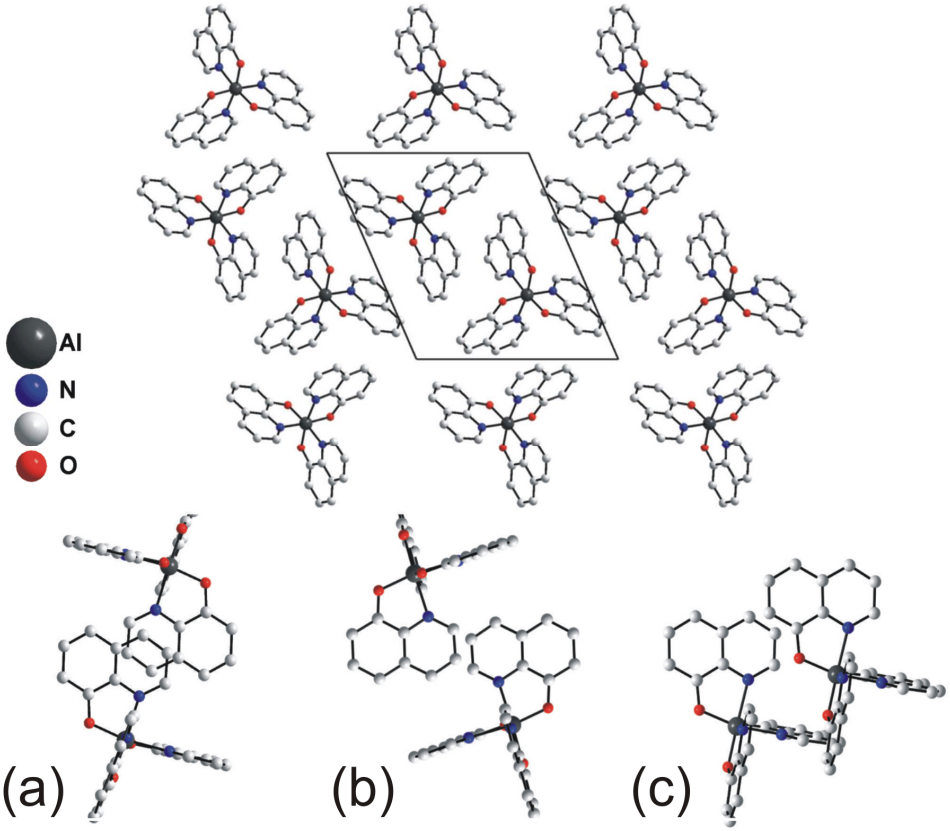

Figure 14: *Crystal structure of δ-Alq_3 in a projection along the c-axis. (a), (b), and (c) are projections perpendicular to the planes of the hydroxyquinoline ligands 1, 2, and 3, respectively, showing the overlap between ligands of neighboring Alq_3 molecules.*

Physics of Organic Semiconductors, W. Bruetting (Ed.), Wiley-VCH (2005) 95-127 https://doi.org/10.1002/3527606637.ch4

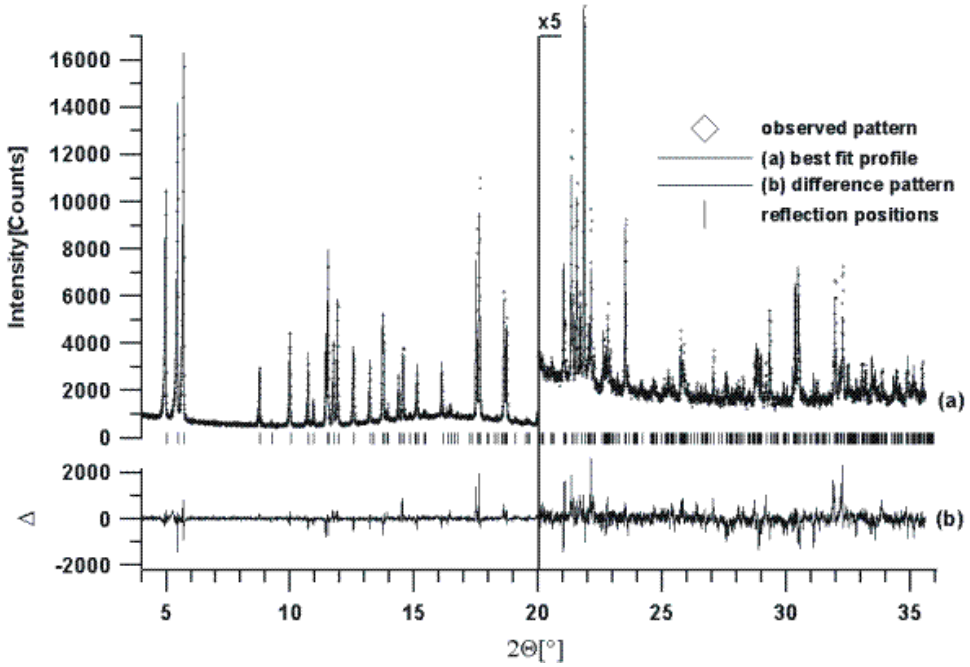

Figure 15: *Scattered X-ray intensity for δ-Alq_3 at ambient conditions. Shown are the observed patterns (diamonds), the best Rietveld-fit profiles on the assumption of a meridional isomer (line) and the enlarged difference curves between observed and calculated profiles in an additional window below. Best values obtained for R_p, R_{wp} and R-F^2 are 7.3%, 9.4% and 19.4%, respectively.*

facial isomer at elevated temperature is possible, as was carried out for the δ-phase.
Brinkman et al. used the preparation method that is described in this review to obtain different phases of Tris(8-hydroxyquinoline) Gallium(III) [33]. It is highly remarkable, that they observed the same behavior as we describe here for Alq_3. Thus it is not simply related to the Alq_3 molecule but seems to be a general property of this class of chelate complexes.

Vibrational Analysis

Due to the different molecular symmetry of the meridional and facial isomers (C_1 versus C_3), vibrational analysis using infrared (IR) spectroscopy should be another possible method to differentiate between them. In particular, the first coordination sphere or central part of the molecule AlO_3N_3 should show characteristic vibrational properties for each isomer (Al-O and Al-N modes located below 600cm^{-1}, as calculated by Kushto et al. [25]). Furthermore, there is a weak coupling of the three ligands via the central part, and movements around the central aluminum atom are involved in most of the molecular vibrations below 1700cm^{-1}. This coupling depends on the relative positions of the oxygen atoms of the ligands (compare Fig. 2). For the facial isomer each oxygen atom faces a nitrogen atom, and thus the coupling via the Al atom is identical for all ligands, whereas for the meridional isomer one can clearly distinguish between the ligands labeled by A, B and C in Figure 2. For the meridional isomer, the coupling mainly affects the ligands B and C, where the oxygen atoms face each other, and to a lesser extent the A and B ligands, which have the oxygen and nitrogen atoms opposite. The coupling mechanism of ligand A and C is mainly characterized by the modes of the two opposite nitrogen atoms. This means that due to the

Physics of Organic Semiconductors, W. Bruetting (Ed.), Wiley-VCH (2005) 95-127 https://doi.org/10.1002/3527606637.ch4

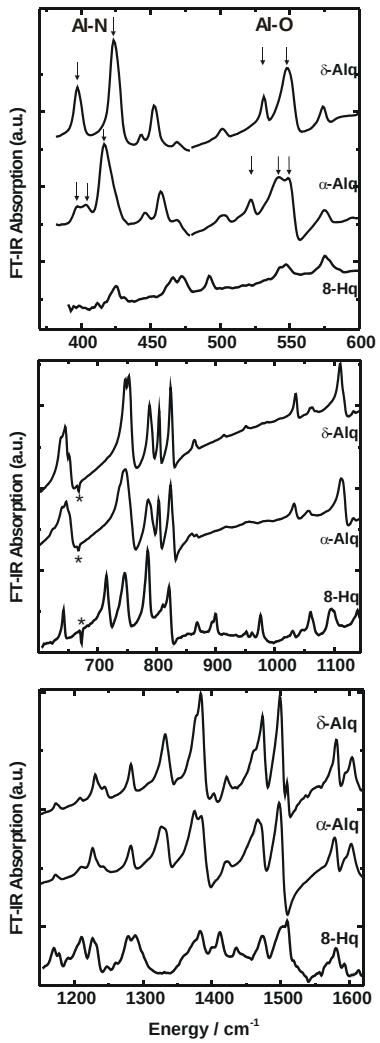

Figure 16: *Comparison of the FTIR-spectra of δ-Alq_3 (upper trace), α-Alq_3 (middle trace) and hydroxyquinoline (8-Hq, lower trace) in the range from 350cm^{-1} to 1650cm^{-1}*

lower symmetry of the meridional molecule each vibrational mode has a slightly different energy for the three ligands.

For the δ-phase of Alq_3 it was shown above by structural investigations to consist of the facial isomer. We can therefore use the IR spectra to identify characteristic differences in the vibrational properties of the two isomers. Figure 16 shows a comparison of the FT-IR-spectra of δ-Alq_3, α-Alq_3, and the ligand hydroxyquinoline (8-Hq) alone. In principle one has to distinguish between two regions, above and below 600cm^{-1}. The lines above 600cm^{-1} are mainly related to vibrations within the ligands, as one can see from comparison with the 8-Hq spectrum. Due to the different symmetry of the isomers there is a different interaction of the ligands via the Al-atom leading to small differences in this region. The region below 600cm^{-1} is dominated by the modes of the first coordination sphere or central fragment around the Al-atom. A detailed discussion of these spectra and individual lines as well as a discussion of the influence of crystallinity of the sample can be found in Refs [47, 52]. In this review we only give the main

Physics of Organic Semiconductors, W. Bruetting (Ed.), Wiley-VCH (2005) 95-127 https://doi.org/10.1002/3527606637.ch4

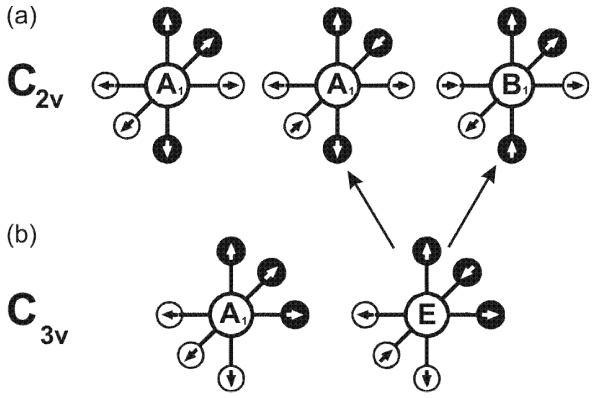

Figure 17: *Schematic picture of the central part of the meridional (a) and the facial (b) isomer of Alq_3. Hollow and filled circles around the central Al-atom represent oxygen and nitrogen atoms, respectively. The three stretching modes of the meridional molecule (C_{2v}-symmetry) and the two for the facial molecule (C_{3v}-symmetry, one is degenerated) are marked by arrows in the O and N atoms.*

results and exemplify the discussion by the Al-N and Al-O stretching modes that are marked with arrows in Figure 16.

If we consider the central fragment AlO_3N_3, the local symmetry for each isomer is C_{2v} and C_{3v}, respectively, as shown in Figure 17. The separation of the central part from the ligands is justified by the different and well-separated vibrational energies belonging to these groups, as observed in the comparison of Alq_3 with the hydroxyquinoline parent of the ligands in Figure 16. Particular focus is on the stretching vibrations of this central part. For α-Alq_3, which consists of the meridional isomer (C_{2v}), six stretching vibrations are expected, three involving Al-N and three involving Al-O modes (see Figure 17). As they are all dipole-allowed, they are observable by IR-spectroscopy. According to Kushto et al. the following assignments for α-Alq_3 are made: Al-N stretching: 396cm^{-1}, 405cm^{-1}, 418cm^{-1}, Al-O stretching: 522cm^{-1}, 542cm^{-1}, 549cm^{-1}. By contrast δ-Alq_3 shows a total of only four bands in this region (397cm^{-1}, 423cm^{-1}, 531cm^{-1}, 548cm^{-1}). As the AlO_3N_3 fragment of the facial isomer belongs to symmetry C_{3v}, six stretching vibrations are expected here too, but four of them belong to two degenerate vibrational states and therefore only four bands should be observed in IR-spectroscopy, as is the case for δ-Alq_3. The Al-N stretching is found at 397cm^{-1} and 423cm^{-1}, the Al-O stretching at 531cm^{-1} and 548cm^{-1}. The degeneracy of the first and last band is not present in the α-phase of Alq_3 (see Figure 16 and Figure 17), which consists of the meridional isomer. Two lines are observed at 400cm^{-1} and at 550cm^{-1} in α-Alq_3, in agreement with theoretical calculations of Kushto et al.[25] From this and the discussion in Ref [47] it can be seen, that the analysis of the IR-spectra for the region above as well as below 600cm^{-1} confirms the presence of the meridional and facial isomer in α-Alq_3 and δ-Alq_3, respectively. Furthermore, the specific fingerprints of the two isomers obtained by IR-spectroscopy may help to identify the isomers in other Alq_3-samples [47].

Population and properties of the electronic excited triplet state

Population of the triplet states

In the previous part of this review structural investigations and properties of the molecule in the electronic ground state were discussed, giving evidence for the existence of the two different geometric isomers. However, not only the electronic ground state should be different for the two isomers, but also the excit-

Physics of Organic Semiconductors, W. Bruetting (Ed.), Wiley-VCH (2005) 95-127 https://doi.org/10.1002/3527606637.ch4

ed states are expected to have different properties due to the different geometry of the molecule. Two types of photoexcited states are distinguished: the singlet state and the triplet state. In the singlet state the total spin quantum number of the unpaired electrons S=0, whereas in the triplet state the total spin quantum number is S=1.

As in most cases the S_0-S_1 transition is an allowed transition, the lifetime of the S_1-state is very short. For Alq_3 it was measured to be about 12ns [3, 29, 53, 54]. On the other hand, the S_0-T_1 transition is a so-called forbidden transition and thus the lifetime of the T_1 state is expected to be several orders of magnitude larger. However, so far very few experimental data on the triplet state of Alq_3 have been available, and thus this section includes the first direct measurements of the triplet state. First, a method to investigate the population of the triplet states due to intersystem crossing (ISC) is introduced and applied to discuss the properties of the different phases. Then we briefly discuss very recent results related to the characterization of the electronic excited triplet state in Alq_3.

The triplet state T_1 is populated due to intersystem crossing, as schematically shown in Figure 18. In reality the triplet state splits into three levels |x>, |y> and |z>. Their energetic distance is characterized by the zero field splitting parameters E and D. To simplify the following discussion this splitting of the triplet state is neglected and only T_1 is given in the schematic Figure 18. Due to photoexcitation by the absorption of incident laser light, mainly the singlet states S_n are excited ($S_0 \rightarrow S_n$) and relax to the lowest excited singlet state S_1 (process a). The excited singlet state S_1 can relax to the ground state ($S_1 \rightarrow S_0$) by emission of a photon (process b) or simply relax thermally (process c). The triplet state is populated by intersystem crossing with the rate constant d and f is the rate constant for the $T_1 \rightarrow S_0$ transition. In the literature f is often denoted as k_T.

Under constant photoexcitation and for long periods of time ($t \rightarrow \infty$) there is a dynamic equilibrium of the $S_1 \rightarrow T_1$ and $T_1 \rightarrow S_0$ transitions, resulting in a constant concentration of the triplet states $[T_1]^\infty$. The molecules which are in the long-lived triplet state are not able to emit fluorescent light and, at high excitation density, this leads to a decrease in fluorescence intensity. Therefore the process of intersystem crossing can be investigated by transient PL measurements and as a result the ratio of molecules in the triplet state can be estimated. The time dependence of the population process and the concentration of the triplet states $[T_1]^\infty$ is obtained from the rate equations (see Figure 18):

$$\frac{d[S_0]}{dt} = -a[S_0] + b[S_1] + c[S_1] + f[T_1] \tag{1}$$

$$\frac{d[S_1]}{dt} = a[S_0] - b[S_1] - c[S_1] - d[S_1] \tag{2}$$

$$\frac{d[T_1]}{dt} = d[S_1] - f[T_1] \tag{3}$$

These equations were solved by Sveshnikov, and Smirnov et al. [55, 56]. As the rate constants *b* and *c* cannot be distinguished experimentally here, they can be replaced by $b' = b + c$. Further, if we bear in mind both that the lifetime of the triplet state is much longer than the lifetime of the singlet state and that the rate of intersystem crossing is much higher than the rate of triplet decay ($b' >> f$, $d >> f$), the solutions are

$$[S_1] = \frac{af[S_0]^0}{(b'+d)f + da} + \frac{Aa^2[S_0]^0}{(b'+d)f + da} e^{-\frac{1}{\tau_1}t} - \frac{a[S_0]^0}{b'+d+Ba} e^{-\frac{1}{\tau_2}t} \tag{4}$$

$$[T_1] = \frac{ad[S_0]^0}{(b'+d)f + da}\left(1 - e^{-\frac{1}{\tau_1}t}\right) \tag{5}$$

Physics of Organic Semiconductors, W. Bruetting (Ed.), Wiley-VCH (2005) 95-127 https://doi.org/10.1002/3527606637.ch4

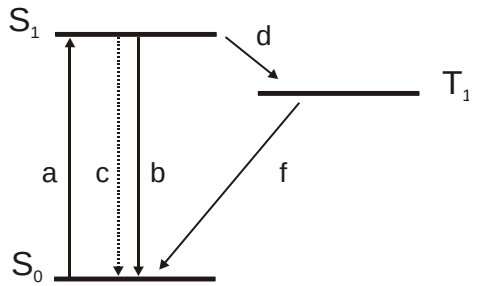

Figure 18: *Schematic diagram of the electron levels and the transitions between the levels in an organic molecule. S_0, and S_1 are the non-excited ground state and the first excited singlet level; T_1 is the lowest triplet level. The coefficient a is proportional to the intensity of the exciting light and the probability of excitation of the molecule. b, c, d and f are the corresponding rate constants. The transition d is the population of the triplet state due to intersystem crossing.*

with

$$f + \frac{d}{b'+d}a = f + Aa = \frac{1}{\tau_1} \tag{6}$$

and

$$b'+d+\frac{b'}{b'+d}a = b'+d+Ba = \frac{1}{\tau_2}. \tag{7}$$

From these equations it is evident that τ_1 is the characteristic time for the accumulation of molecules in the triplet state. For $t\rightarrow\infty$ (stationary regime) the concentration of molecules in the triplet state is given by

$$[T_1]^{\infty} = \frac{ad[S_0]^0}{(b'+d)f + da} = Aa[S_0]^0\tau_1 \tag{8}$$

and finally with equation (6) one can express $[T_1]^{\infty}$ by the characteristic accumulation time τ_1 and the lifetime of the molecules in the triplet state $\tau_0=1/f$.

$$[T_1]^{\infty} = [S_0]^0\left(1-\frac{\tau_1}{\tau_0}\right) \tag{9}$$

As a result it is possible to estimate the ratio of the molecules excited in the triplet state $[T_1]^{\infty}$ from the lifetime τ_0, determined from delayed fluorescence measurements that will be discussed below, and the characteristic accumulation time τ_1, which can be measured using transient PL studies.

Physics of Organic Semiconductors, W. Bruetting (Ed.), Wiley-VCH (2005) 95-127 https://doi.org/10.1002/3527606637.ch4

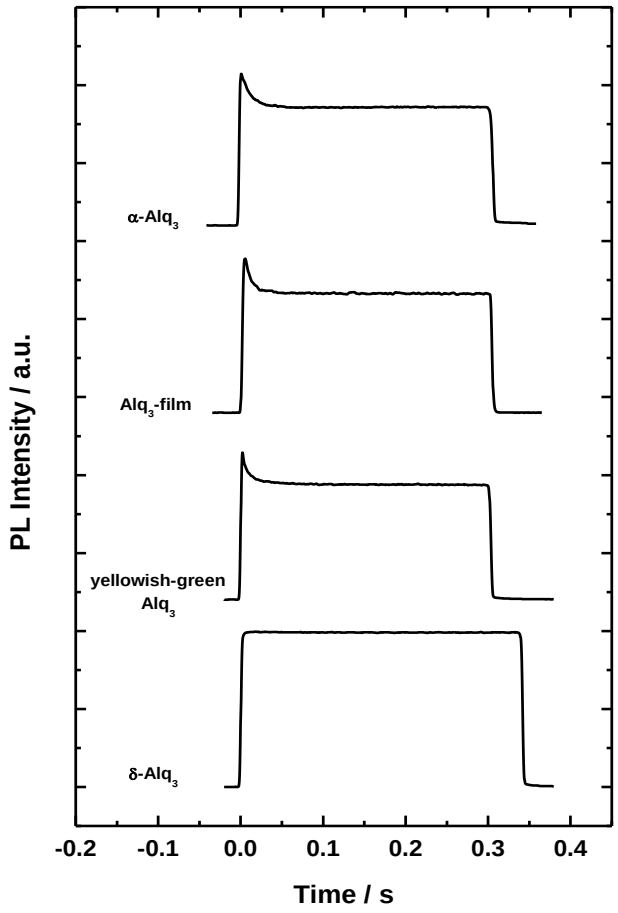

Figure 19: *Time dependence of the PL-intensity during an optical excitation pulse for polycrystalline Alq_3 phases and an evaporated film. The measurements were performed at 1.3K by using excitation at 363.8nm. The signal was detected at 2.64eV (470nm) for δ-Alq_3 and at 2.48eV (500nm) for all other samples.*

These measurements for the Alq_3 phases as well as for an evaporated amorphous film are shown in Figure 19. Instantaneously with the turning-on of the excitation light the fluorescence is observed, which subsequently decreases with a decay time τ_1 to an equilibrium value. α-Alq_3, yellowish-green Alq_3 and the evaporated amorphous film behave in a similar fashion. Their decay time τ_1 is 11ms, 11ms, and 7ms, and the triplet lifetime τ_0 at that temperature (1.3K) was measured as 15ms, 14ms, and 9ms respectively. Therefore in these samples about 20% to 30% of the molecules are in the triplet state. This similarity between these samples of Alq_3 containing the meridional isomer is remarkable, because it clearly demonstrates that the morphology and thus intermolecular interactions seem to have no significant influence on the intersystem crossing process in Alq_3. However, for δ-Alq_3 there is only a very small decrease in the PL intensity and the equilibrium value remains at 98%. Due to the small decay and the noise of the measurement, the error for determination of τ_1 is too large, but from the decrease in intensity one may roughly estimate that only about 2% of the molecules in δ-Alq_3 are in the triplet state. From the independence of the morphology of the samples it can be concluded that the low population of the triplet state due to strongly reduced intersystem crossing is a molecular property of the facial isomer in δ-Alq_3. This has also been confirmed recently by Amati et al. using quantum chemical calculations [57].

Physics of Organic Semiconductors, W. Bruetting (Ed.), Wiley-VCH (2005) 95-127 https://doi.org/10.1002/3527606637.ch4

Phosphorescence of Alq_3

The measurement of the transient PL discussed above gives information about intersystem crossing to the triplet state but not about its energetic position and lifetime. Until recently, the determination of the triplet properties has been based on theoretical calculations [24] and only very few experimental data were available so far: for example, the lifetime of the triplet state was derived from measurements of the diffusion length at room temperature using a phosphorescent sensoring layer on the assumption of non-dispersive transport, and the triplet energy was inferred from other metal-chelate complexes [61]. These experimental methods were necessary because no radiative triplet emission of Alq_3 (no phosphorescence) has been found. Only very recently direct observations of the electronic excited triplets have been reported: H.D. Burrows et al. published a phosphorescence spectrum of Alq_3 in an ethyl iodide glass matrix [62]. We measured the electro-phosphorescence of Alq_3-based OLEDs by using delayed electroluminescence [59], further, phosphorescence was also shown for all crystalline phases and for the evaporated amorphous film [52,60,63]. Here we summarize the results that were mainly obtained by delayed fluorescence as well as by phosphorescence of Alq_3.

The zero-field splitting parameters E and D are characteristic values for the triplet state. They were determined by ODMR measurements at zero field [60]. The measured values of the zero-field splitting parameters of $|E|=0.0114$ cm^{-1} and $|D|= 0.0630$ cm^{-1} are in the same range for the crystalline phases (α- and yellowish-green Alq_3) and for evaporated amorphous films, indicating a weak influence of the morphology. Calculations of the zero-field splitting parameters of the meridional Alq_3 molecule, starting from the D and E values of the isolated ligands, seem to support a mini-exciton-like behavior of the triplet state on the three ligands of the Alq_3 molecule [60].

In order to learn more about the properties of the triplet state, measurements of the transient PL in the millisecond time range were taken. From these it is possible to obtain information about the lifetime and the population of the long-lived triplet state due to intersystem crossing. The principle of these measurements is shown in Figure 20. The sample is excited by a rectangular laser pulse (dotted line), and as soon

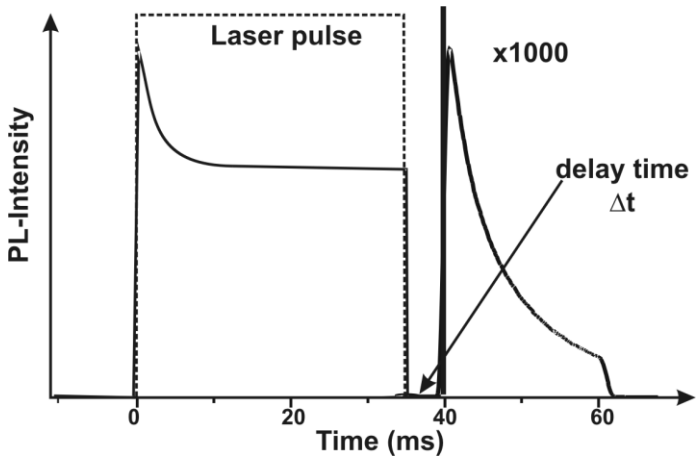

Figure 20: *Principle of the transient PL measurements shown for α-Alq_3 measured at 20 K. By applying an intense rectangular laser pulse, PL from the sample is observed instantaneously. During the first 10-15 ms the PL-signal decreases due to intersystem crossing to a constant equilibrium value. After the laser is turned off, the spontaneous PL decreases within less than 1 μs. The fluorescence observed after the laser has been turned off is called delayed fluorescence, with an intensity of about three orders of magnitude less than the spontaneous PL. In our experiments this delayed fluorescence was measured after a delay time Δt of several milliseconds. The cut-off of the delayed fluorescence, here at about 60 ms, is due to the chopper system of the setup*.

as the excitation light is turned on the spontaneous Alq_3 fluorescence is observed, which subsequently

Physics of Organic Semiconductors, W. Bruetting (Ed.), Wiley-VCH (2005) 95-127 https://doi.org/10.1002/3527606637.ch4

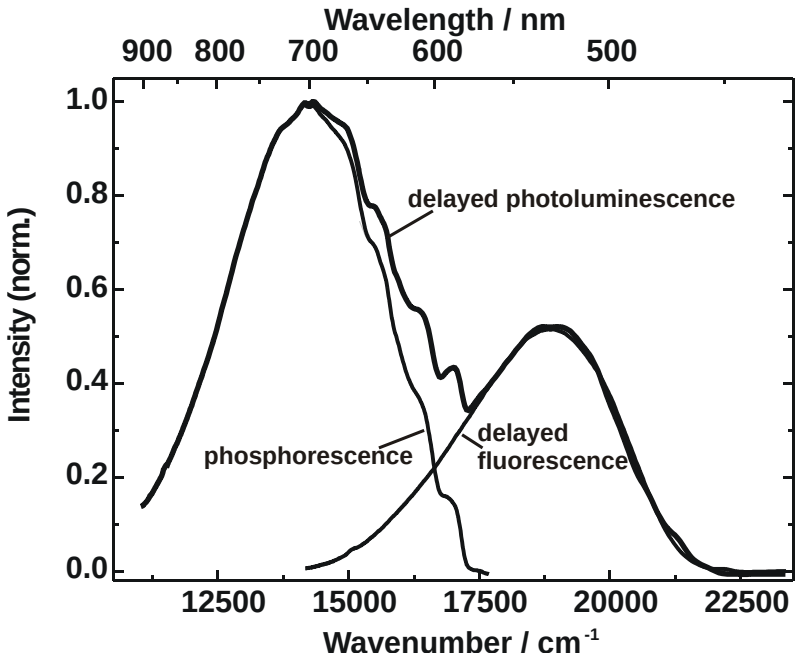

Figure 21: *Delayed PL spectrum of α-Alq_3 at 10 K measured with a delay time Δt of 4ms. Excitation wavelength was 442 nm. The spectrum shows two distinct bands: the typical PL spectrum and a new additional band at about 700 nm (1.77 eV). The band at about 525nm is the delayed fluorescence (DF), the band at about 700nm the phosphorescence of Alq_3.*

decreases to an equilibrium value with a decay time of about 10 ms. This decay is related to the population of the triplet states by ISC as discussed in detail above.

After the laser is turned off, the intensity of spontaneous PL from the singlet states decreases very fast due to their short lifetime of about 10 ns [3,29,53,54] and only the triplet state whose lifetime is often in the range of several milliseconds, is still populated; thus after just 1 μs no spontaneous fluorescence is present any more. However, even after a delay time Δt of 4 ms, a weak PL is still observed. It is about three orders of magnitude less intense than the spontaneous PL and shows a slow decay rate. This process is known as delayed fluorescence (DF) in the literature. It occurs due to collision of two triplet excitations and is therefore a bimolecular process, which has a probability proportional to the square of the density of the triplet states [T_1]. The collision process is also often referred to as triplet exciton fusion or sometimes as T-T annihilation. If the energy of the lowest excited singlet state is less than the sum of the energies of the colliding triplet excitons, the fusion reaction may yield triplet and singlet states. The generated singlet exciton S_1 then decays, as would be the case for a directly excited singlet exciton state. As the DF originates from the $S_1 \rightarrow S_0$ transition, its spectrum is the same as observed in usual PL measurements, only significantly less intense than the instantaneous PL spectrum (in our case the difference is about three orders of magnitude). The distinguishing feature of the fluorescence from the S_1-state gener-

Table 3: *Lifetimes obtained from the transient measurements of I_{DF} of the different polycrystalline Alq_3 phases and amorphous films at a temperature of about 20 K. τ_{DF} is the time constant for the exponential decay of I_{DF} and from this the triplet lifetime τ_0 was obtained. τ_{700} is the time constant of the exponential decay of the luminescence intensity measured at 730 nm.*

	τ_{DF}	τ_0 (=2τ_{DF})	τ_{700}	τ_{700}/τ_{DF}
α-Alq_3	6.6±0.5	13.2±1	13.6±0.5	2.05
Yellowish-green	7.8±0.5	15.6±1	16.2±0.5	2.08
δ-Alq_3	6.2±0.5	12.4±1	13.2±0.5	2.13
Film	4.33±0.5	8.66±1	9.3±0.5	2.15

Physics of Organic Semiconductors, W. Bruetting (Ed.), Wiley-VCH (2005) 95-127 https://doi.org/10.1002/3527606637.ch4

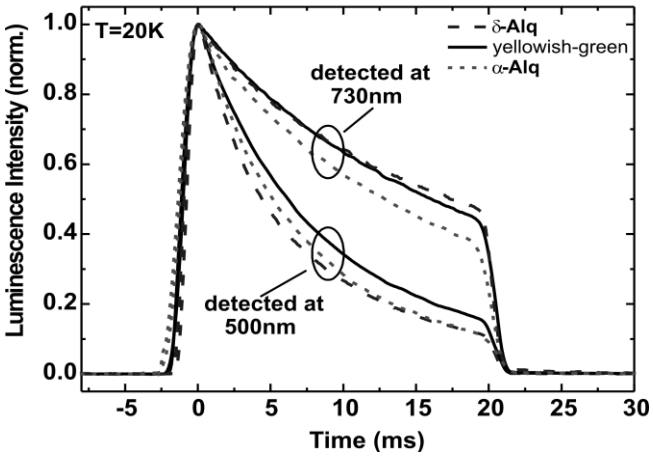

Figure 22*: Transient intensity of the delayed luminescence shown in Figure 5 detected at 500 nm and at 730 nm, respectively. The delay time Δt was 4 ms in all cases. The steep edge at 20 ms is due to the experimental setup. The temperature was 20 K.*

ated by the fusion process is that its apparent lifetime is determined by the triplet excitons and hence is much longer than the lifetime of the spontaneous fluorescence.

Figure 21 shows the delayed PL spectrum of α-Alq_3 at 10 K measured with a delay time Δt of 4 ms and the spectrum was integrated over about 20 ms. It shows two distinct bands, one at about 500 nm, similar to spontaneous PL, and an additional band at about 700 nm. For α-Alq_3, yellowish-green Alq_3 and the evaporated film the position of the bands is approximately the same, whereas for δ-Alq_3 the bands are slightly blue-shifted. The relative intensity of the two bands is different for the different phases and temperature-dependent [64]. As the excitation wavelength of 442 nm is located below the absorption edge of δ-Alq_3, the obtained density of excited states is significantly lower for δ-Alq_3. Under these experimental conditions only a very weak band at 500 nm was observed for δ-Alq_3 due to the low density of triplet

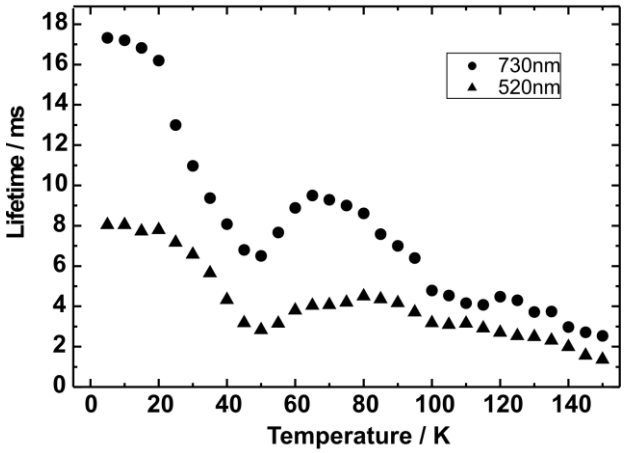

Figure 23: *Lifetimes of both bands of the delayed PL of yellowish-green Alq_3-powder shown in Figure 2 in a temperature range between 6 K and 150 K. The lifetimes of both bands increase with decreasing temperature but show a local minimum at about 50K that is assigned to a phase transition [60,64].*

Physics of Organic Semiconductors, W. Bruetting (Ed.), Wiley-VCH (2005) 95-127 https://doi.org/10.1002/3527606637.ch4

states, but the band at 700 nm was still clearly resolved [52,60,64].
The vibronic progressions on the high energy side of the band at 700 nm are clearly resolved. By subtraction of the usual PL spectrum from the delayed PL spectrum bands at 700 nm with vibronic progressions are obtained as shown for α-Alq in Figure 21. These are at approximately the same positions for α-Alq_3 and yellowish-green Alq_3. The vibronic progressions for α-Alq_3 and yellowish-green Alq_3 are located at about 586 nm, 606 nm, 627 nm, 645 nm and 668 nm (17065 cm^{-1}, 16502 cm^{-1}, 15950 cm^{-1}, 15504 cm^{-1} and 14970 cm^{-1}), and for δ-Alq_3 at about 574nm, 594 nm, 613 nm and 635 nm (17422 cm^{-1}, 16835 cm^{-1}, 16313 cm^{-1} and 15748 cm^{-1}), and thus have an average distance of about 550 cm^{-1}, similar to the vibronic progression observed for the PL [15]. For the amorphous film the distance between the vibrational modes are similar but their position seems to be slightly red-shifted as reported in Refs [59,63]. The vibrational modes of the new band at about 700 nm are due to the vibrational modes of the Alq_3 molecule in its electronic ground state.
Later on it is shown, that the new band at about 700 nm is the $T_1 \rightarrow S_0$ transition. As this phosphorescence spectrum shows well-resolved vibronic progressions, one can directly determine the triplet energy by assignment of the lowest resolved vibronic band to the 0-0 transition. Hence the triplet energy for the meridional isomer (in α-Alq_3) can be determined as 2.11±0.1 eV and for the facial isomer (in δ-Alq_3) as 2.16±0.1 eV. For the evaporated film the lowest resolved vibronic progression seems to be slightly red-shifted [60,63] These experimental values are similar to the values roughly estimated by Baldo et al. (2 eV)[61], are very close to the theoretical value calculated by Martin et al. for an isolated molecule (2.13 eV) [24] and also close to the triplet energy of 2.17±0.1 eV that has been estimated from the phosphorescence spectrum of Alq_3 in an ethyl iodine glass matrix [62].
The transient PL intensity of both bands was also investigated. By measuring the decay of the intensity of the DF (I_{DF}), the lifetime of the triplet states can be determined [52,60,65]. For this one has to distinguish between two regimes, namely high and low triplet concentration. At very high triplet densities the T-T-annihilation directly influences the lifetime of the triplets in the sample and therefore the regime of low concentration has to be chosen to measure the correct triplet lifetime τ_0. This is equivalent to ($k_T[T_1] >> \gamma_{tot}[T_1]^2$), where k_T is correlated with the triplet lifetime τ_0 by ($\tau_0 = 1/k_T$) and γ_{tot} is the total bimolecular annihilation (fusion) rate constant. In this case I_{DF} decays according to a monoexponential law $I_{DF}(t) \sim e^{-2k_T t}$ The decay time of I_{DF} is half of the correlated triplet lifetime τ_0, and thus it is possible to

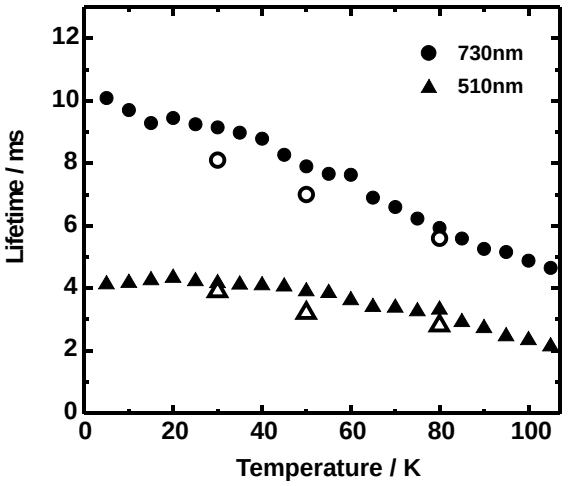

Figure 24:*Lifetimes of both bands of the delayed PL of an evaporated amorphous film (thickness 5 μm) over a temperature range of 100 K. Delay time Δt was 4 ms, the detection wavelengths were 510 nm and 730 nm, respectively. Hollow symbols indicate values measured by delayed electroluminescence of an Alq_3-LED which lead approximately to the same results as measurements using photoexcitation [59,63].*

Physics of Organic Semiconductors, W. Bruetting (Ed.), Wiley-VCH (2005) 95-127 https://doi.org/10.1002/3527606637.ch4

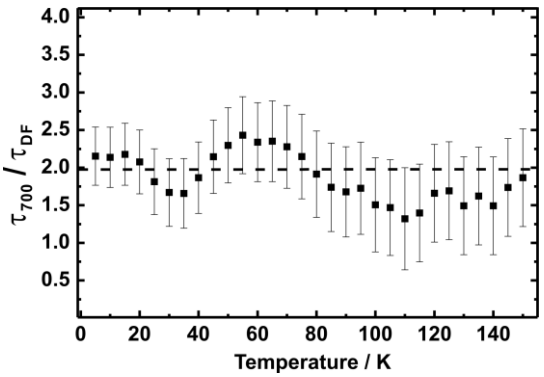

Figure 25: *Temperature dependence of the factor (τ_{700}/τ_{DF}) between the decay times measured for the DF at 500 nm (τ_{DF}) and for the band at 700 nm (τ_{700}) of yellowish-green Alq_3-powder. The dashed line at the factor(τ_{700}/τ_{DF})=2 serves as a guide to the eye. From theory the lifetime of the DF should be half of the lifetime of the phosphorescence. Within the accuracy of the measurement τ_{700} and τ_{DF} are very well correlated by a factor of 2 over a wide range of temperatures, which confirms the assignment of the band at 700 nm to the phosphorescence of Alq_3.*

determine the lifetime of the triplet state by transient measurements of I_{DF}. By choosing the delay time Δt to be at least 4 ms we obtained very good monoexponential decays of the DF detected at 500 nm, confirming that the measurements were in the correct regime.

Figure 22 shows the intensity decay of the delayed luminescence of polycrystalline samples detected at 500 nm and of the additional band detected at 730 nm and measured at a temperature of 20 K. The measured apparent lifetimes of the delayed fluorescence detected at 500 nm are 6.6 ±0.5 ms, 7.8±0.5 ms and 6.2±0.5 ms, resulting in triplet lifetimes of 13.2±1 ms, 15.6±1 ms and 12.4±1 ms for α-Alq_3, yellowish-green Alq_3 and δ-Alq_3, respectively. The values are summarized in Table 3. Although in the film the triplet lifetime is about 60% - 70% of that in the polycrystalline samples, all values are in the same range and thus the morphology of the samples seems to have only little influence on the lifetime of the triplet states.

The decay of the band at about 700 nm is also shown in Figure 22. All polycrystalline phases show a similar monoexponential decay, which is significantly slower than that detected at 500 nm. Measured monoexponential decay times are also given in Table 3. Within the accuracy of the measurement these values are about a factor of 2 higher than the values for the band at 500 nm and thus almost identical to the triplet lifetimes obtained.

The temperature dependence of the decay of both bands was investigated for all phases of Alq_3 including amorphous thin films, and as a result it became clear that both bands are directly correlated [52,60,64]. In principle the lifetime of the delayed fluorescence and the band at 700 nm increases with decreasing temperature, as shown in Figure 23 for yellowish-green Alq_3 powder. A local minimum is observed at about 50 K. This is due to a reversible phase transition that we also observed in temperature-dependent PL quantum efficiency measurements and ESR measurements[66]. Similar behavior was observed for δ-Alq_3 and amorphous films. For the evaporated amorphous film the local minimum is located at about 100 K (Figure 24). Measurements of the delayed fluorescence and phosphorescence of Alq_3-based OLEDs gave similar values and are also included for comparison [59]. As shown in Figure 25 for yellowish-green Alq_3-powder and in Figure 26 for the evaporated film, the lifetime of the band located at about 700 nm and the apparent lifetime of the delayed fluorescence always differ by a factor of 2 within the accuracy of the measurements, and thus the lifetime of this band is identified to be the lifetime of the triplet state. Therefore it is obvious that the band at 700 nm is directly linked with the triplet state of Alq_3. This justifies the assignment of this band to the $T_1 \rightarrow S_0$ transition and thus this spectrum is the phosphorescence spectrum of Alq_3.

Physics of Organic Semiconductors, W. Bruetting (Ed.), Wiley-VCH (2005) 95-127 https://doi.org/10.1002/3527606637.ch4

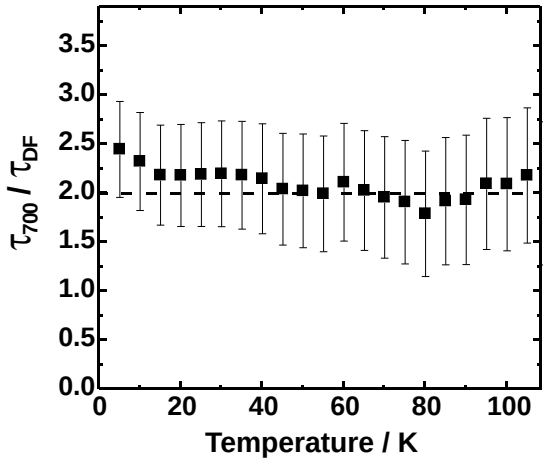

Figure 26: *Factor (τ_{700}/τ_{DF}) between the decay times measured for the delayed fluorescence at 500 nm (τ_{DF}) and for the band at 700 nm (τ_{700}) of the Alq_3 film. The dashed line at the factor (τ_{700}/τ_{DF})=2 serves as a guide to the eye. The lifetimes of both bands are correlated by a factor of 2.*

Summary

In this review we have presented detailed investigations on polycrystalline Alq_3-samples prepared using sublimation in a horizontal glass tube with a temperature gradient or by annealing. The thermal, structural and photophysical properties were investigated by using differential scanning calorimetry (DSC), X-ray diffraction, infrared spectroscopy, and photoluminescence measurements, with the focus on the comparison of the different phases.

It was shown that different fractions of Alq_3 can be separated in the sublimation tube; they differ in the shape of the crystals, their color, their solubility, and their fluorescence. An important outcome was the discovery of a new blue luminescent crystalline phase of Alq_3 (δ-Alq_3), which has significantly different properties compared to all other known phases (α, β, γ). Furthermore, it was demonstrated that the material commonly used for the evaporation of thin films in OLEDs (here named yellowish-green Alq_3) mainly consists of α-Alq_3 with some small admixtures of δ-Alq_3.

As temperature has a strong influence on the formation of these polycrystalline phases, the formation conditions of the different phases of Alq_3 were investigated using differential scanning calorimetry measurements in combination with structural and optical characterization. As a result a phase transition at about 380°C was identified where blue luminescent Alq_3 is formed. From detailed investigations of the processes in the temperature region between 385°C and 410°C, the two high-temperature phases δ-Alq_3 and γ-Alq_3 were identified. In addition, an efficient method was developed to prepare large amounts (several grams) of pure blue luminescent δ-Alq_3. It was also shown that all phases can easily be transformed into each other; thus chemical reactions could be excluded.

Well-defined preparation of pure δ-Alq_3 was the prerequisite for high resolution X-ray measurements on δ-Alq_3 powder including structural refinements. The high quality of these refinements gave convincing evidence that the facial isomer constitutes the δ-phase of Alq_3. The data also provided information about distance and orientation of the molecules and thus about molecular packing in the crystal. Compared to the α- and β-phase, both consisting of the meridional isomer, a strongly reduced π-orbital overlap of hydroxyquinoline ligands belonging to neighboring Alq_3 molecules was found in δ-Alq_3. Therefore both

Physics of Organic Semiconductors, W. Bruetting (Ed.), Wiley-VCH (2005) 95-127 https://doi.org/10.1002/3527606637.ch4

the packing effect with reduced intermolecular interaction and the changed symmetry of the molecule are likely to be responsible for the large blue-shift of the photoluminescence.
Using infrared spectroscopy it was demonstrated how the isomerism of the Alq_3 molecule is manifested in the vibrational properties. Comparison of the experimental results with theoretical calculations provided further evidence of the presence of the facial isomer in the blue luminescent δ-phase of Alq_3.
Experiments on other chelate complexes [33] suggest that the structural and thermal properties described for Alq_3 in this review are general properties of this class of chelate complexes.
Finally this article presented first results of the electronic excited triplet state in Alq_3. The intersystem crossing behavior was investigated, the phosphorescence spectrum was measured and it was found that the reduced population of the triplet states in δ-Alq_3 due to intersystem crossing is a characteristic property of the facial isomer.
Although Alq_3 is a so called singlet-emitter it is possible to characterize its triplet state and to measure the radiative $T_1 \rightarrow S_0$ transition, the phosphorescence. This was shown for different morphologies: crystalline phases, amorphous films and of diluted material in a frozen glass matrix. The delayed luminescence of the crystalline phases and the amorphous films shows two distinct bands: the delayed fluorescence and the phosphorescence of Alq_3. The data obtained for the amorphous films are in very good agreement with the data reported for Alq_3-based OLEDs. Well-resolved vibrational progressions for all samples allowed a precise determination of the triplet energy, namely 2.11±0.1 eV and 2.16±0.1eV for the meridional isomer (in α-Alq_3) and facial isomer (δ-Alq_3), respectively. Temperature-dependent investigations of the delayed luminescence in the range between 6K and 150K confirmed the identification of the phosphorescence band since the lifetime of the delayed fluorescence and of the phosphorescence always differ by a factor of two, as expected from theory. The triplet lifetime shows a clear temperature dependence from about 17 ms at 6 K to 4 ms at 120 K for yellowish-green Alq_3. These measurements also indicated a phase transition of Alq_3 at about 50 K. This direct characterization of the triplet state in Alq_3 is highly relevant for applications such as Alq_3-based OLEDs as most of the excitons formed in OLEDs are triplet excitons.
With regard to the application of Alq_3 in OLEDs, it is important to note that the simple annealing process can be used to obtain thin films of blue luminescent Alq_3. In preliminary experiments evaporated amorphous thin films with thicknesses from 300nm to 15µm, were encapsulated and converted at 390°C into thin films showing blue luminescence. In addition it was possible to evaporate blue luminescent thin films directly onto heated glass substrates. At present, these films are still comparatively thick (several microns), have polycrystalline structure, and need further optimization. This would then allow OLEDs to be manufactured with blue luminescent Alq_3. Further work to characterize such films and their application in OLEDs is in progress.

Acknowledgements

The authors would like to thank all those that made this work possible. In particular we would like to thank Jürgen Gmeiner for the preparation of the Alq_3-samples, Markus Braun, Oliver Wendland and Jost-Ulrich von Schütz for transient PL-measurements, Falko D. Meyer, Wolfgang Milius and Harald Hillebrecht for X-ray analysis, Robert E. Dinnebier for performing the measurements and analysis of the synchrotron data, Stefan Forero-Lenger for IR-measurements, Marian Tzolov for Raman measurements that confirmed the IR-data, Christoph Gärditz for measurements of the delayed luminescence and, last but not least, Thomas Stübinger, Anton G. Mückl and Markus Schwoerer for helpful discussions.

References

[1] W. Ohnesorge, and L. Rogers, Spectrochim. Acta, Part A **15**, 27 (1959).
[2] C. Tang, and S. VanSlyke, Appl. Phys. Lett. **51**, 913 (1987).
[3] C. Tang, and S. VanSlyke, J. Appl. Phys. **65**, 3610 (1989).
[4] J. Shi, and C. Tang, Appl. Phys. Lett. **70**, 1665 (1997).
[5] L. Hung, C. Tang, and M. Mason, Appl. Phys. Lett. **70**, 152 (1997).

Physics of Organic Semiconductors, W. Bruetting (Ed.), Wiley-VCH (2005) 95-127 https://doi.org/10.1002/3527606637.ch4

[6] H. Aziz, Z. Popovic, N.-X. Hu, A. Hor, and G. Xu, Science **283**, 1900 (1999).
[7] H. Kubota, S. Miyaguchi, S. Ishizuka, T. Wakimoto, J. Funaki, Y. Fukuda, T. Watanabe, H. Ochi, T. Sakamoto, T. Miyake, M. Tsuchida, I. Ohshita, and T. Tohma, J. Lumin. **87-89**, 56 (2000).
[8] T. Tsutsui, M. Yang, M. Yahiro, K. Nakamura, T. Watanabe, T. Tsuji, Y. Fukuda, T. Wakimoto, and S. Miyaguchi, Jpn. J. Appl. Phys. 2 **38**, 1502 (1999).
[9] P. Burrows, Z. Shen, V. Bulovic, D. McCarty, S. Forrest, J. Cronin, and M. Thompson, J. Appl. Phys. **79**, 7991 (1996).
[10] S. Barth, U. Wolf, H. Bässler, P. Müller, H. Riel, H. Vestweber, P. Seidler, and W. Rieß, Phys. Rev. B **60**, 8791 (1999).
[11] M. Stößel, J. Staudigel, F. Steuber, J. Blässing, J. Simmerer, and A. Winnacker, Appl. Phys. Lett. **76**, 115 (2000).
[12] W. Brütting, S. Berleb, and A. Mückl, Organic Electronics **2**, 1 (2001).
[13] S. Berleb, and W. Brütting, Phys. Rev. Lett. **89**, 286601 (2002).
[14] M. Brinkmann, G. Gadret, M. Muccini, C. Taliani, N. Masciocchi,, and A. Sironi, J. Am. Chem. Soc. **122**, 5147 (2000).
[15] M. Braun, J. Gmeiner, M. Tzolov, M. Cölle, F. Meyer, W. Milius, H. Hillebrecht, O. Wendland, J. von Schütz, and W. Brütting, J. Chem. Phys. **114**, 9625 (2001).
[16] M. Cölle, R.E. Dinnebier, and W. Brütting, Chem. Comm. **23**, 2908 (2002).
[17] M. Cölle, J. Gmeiner, W. Milius, H. Hillebrecht, and W. Brütting, Adv. Funct. Mater. **13**, 108 (2003).
[18] G. Kauffmann, Coord. Chem. Rev**. 12**, 105 (1974).
[19] R. Larsson, and O. Eskilsson, Acta Chem. Scand. **22**, 1067 (1968).
[20] B.C. Baker, and D.T. Sawyer, Anal. Chem. **40**, 1945 (1968).
[21] J. Majer, and M. Reade, Chem. Comm. **1**, 58 (1970).
[22] M. Halls, and R. Aroca, Can. J. Chem. **76**, 1730 (1998).
[23] N. Johansson, T. Osada, S. Stafström,W. Salaneck, V. Parente., D. dos Santos, X. Crispin, and J. Brédas J. Chem. Phys. **111**, 2157 (1999).
[24] R. Martin, J. Kress, I. Campbell, and D Smith, Phys. Rev. B **61**, 15804 (2000).
[25] G. Kushto, Y. Iizumi, J. Kido, and Z. Kafafi, J. Phys. Chem. A **104**, 3670 (2000).
[26] M. Ichikawa, H. Yanagi, Y. Shimizu, S. Hotta, N. Suganuma, T. Koyama, and Y. Taniguchi, Adv. Mater. **14**, 1272 (2002).
[27] R.J. Curry, W.P. Gillin, J. Clarkson, and D.N. Batchelder, J. Appl. Phys. **92**, 1902 (2002).
[28] A. Curioni, M. Boero, and W. Andreoni, Chem. Phys. Lett. **294**, 263 (1998).
[29] W. Humbs, H. Zhangand M. Glasbeek, Chem. Phys. **254**, 319 (2000).
[30] J. Steiger, R. Schmechel, and H. von Seggern, Synth. Met. **129**, 1 (2002).
[31] E. Ito, Y. Washizu, N. Hayashi, H. Ishii, N. Matsuie, K. Tsuboi, Y. Ouchi, Y. Harima, K. Yamashita, and K. Seki, J. Appl. Phys. **92**, 7306 (2002).
[32] M. Amati, and F. Lelj, J. Phys. Chem. A. **107**, 2560 (2003).
[33] M. Brinkmann, B. Fite, S. Pratontep, and C. Chaumont, Chem. Mat. in press.
[34] L.S. Sapochak, A. Padmaperuma, N. Washton, F. Endrino, G.T. Schmett, J. Marshall,D. Fogarty, and S.R. Forrest J. Am. Chem. Soc. **123**, 6300 (2001).
[35] Mettler-Toledo, User Com **11**, 4 (2000).
[36] B. Wunderlich. (1990). *Thermal Analysis*. Academic Press, San Diego.
[37] J. Ford, and P. Timmins, (1989). *Pharmaceutical Thermal Analysis*.
[38] K. Naito, and A. Miura., J. Phys. Chem. **97**, 6240 (1993).
[39] H. Rietveld, J. Appl. Cryst. **2**, 65 (1969).
[40] L. Langford, and D. Louer, Rep. Prog. Phys. **59**, 131 (1996).
[41] R. Young, and D. Wiles J. Appl. Cryst. **15**, 430 (1982).
[42] R.J. Hill, and R.X. Fischer, J. Appl. Cryst. **23**, 462 (1990).
[43] W. Massa, (2000). *Crystal structure determination*. Springer, Berlin.
[44] R. Young (1993). *The Rietveld Method*. Oxford University Press, New York.
[45] P. Coppens, (1992). *Synchrotron Radiation Crystallography*. Academic Press, London.
[46] J.W. Visser., J. Appl. Cryst. **2**, 89 (1969).
[47] M. Cölle, S. Forero-Lenger, J. Gmeiner, and W. Brütting, Phys. Chem. Chem. Phys. **5**, 2958 (2003).
[48] M. Amati, and F. Lelj, Chem. Phys. Lett. **363**, 451 (2002).
[49] M. Utz, C. Chen, M. Morton, and F. Papadimitrakopoulos, J. Am. Chem. Soc. **125**, 1371 (2003).
[50] M. Utz, M. Nandagopal, M. Mathai, and F. Papadimitrakopoulos, Appl. Phys. Lett. **83**, 4023 (2003).
[51] M. Rajeswaran, T.N. Blanton and K.P. Klubek, Z.Kristallogr. NCS **218**, 439 (2003).

Physics of Organic Semiconductors, W. Bruetting (Ed.), Wiley-VCH (2005) 95-127 https://doi.org/10.1002/3527606637.ch4

[52] M. Cölle, (2004). *The Electroluminescent Material Alq_3*, Logos-Verlag, Berlin.
[53] T. Mori, K. Obata, K. Miyachi, T. Mizutani, and Y. Kawakami, Jpn. J. Appl. Phys. 1 **36**, 7239 (1997).
[54] Y. Kawasumi, I. Akai, and T. Karasawa, Int. J. Mod. Phys. B **15**, 3825 (2001).
[55] B. Sveshnikov, Z. Eksp. Teo. Fiz. **18**, 878 (1948).
[56] V.Smirnov, and M. Alfimov, Kinetika i Kataliz **7**, 583 (1966).
[57] M. Amati and F. Lelj, Chem. Phys. Lett., **358,** 144 (2002)
[58] C.E. Pope and M. Swenberg, (1982), *Electronic processes in organic crystals*. Clarendon Press, Oxford.
[59] M. Cölle, and C. Gärditz, Appl. Phys. Lett., **84**, 3160, (2004).
[60] M. Cölle, C. Gärditz and M. Braun, J. Appl. Phys., in press.
[61] M. A. Baldo and S. R. Forrest, Phys. Rev. B **62**, 10958 (2000).
[62] H.D. Burrows, M. Fernandes, J.S. de Melo, A.P. Monkman, and S. Navaratnam, J. Am. Chem. Soc. **125**, 15310 (2003).
[63] M. Cölle and C. Gärditz, Synth. Met., accepted.
[64] M. Cölle and C. Gärditz, J. Lumin., in press.
[65] W. Kao and K. Hwang, *Electrical Transport in Solids*, Pergamon Press, 1981, Oxford.
[66] M. Cölle *et. al.* manuscript in preparation.
[67] X-ray data can be downloaded from the homepage of R. Dinnebier: http://www.fkf.mpg.de/xray/html/isomers.html